UNIVERSITÄTSKLINIKUM HAMBURG-EPPENDORF

Institut für Immunologie

Institutsdirektor: Prof. Dr. med. Marcus Altfeld

Analysis of T cell development in the human thymus by multicolour flow cytometry

Dissertation

zur Erlangung des Grades eines Doktors der Medizin
an der Medizinischen Fakultät der Universität Hamburg.

vorgelegt von:

Sarah-Jolan Bremer
aus Troisdorf

Hamburg 2021

Angenommen von der Medizinischen Fakultät am: 14.09.2022

Veröffentlicht mit Genehmigung der Medizinischen Fakultät der Universität Hamburg.

Prüfungsausschuss, der Vorsitzende: Prof. Dr. Immo Prinz

Prüfungsausschuss, zweite Gutachterin: Prof. Dr. Eva Tolosa

TABLE OF CONTENTS

Received: 28 January 2021 | Accepted: 12 February 2021

DOI: 10.1002/cyto.a.24326

OMIP

ISAC CYTOMETRY Journal of Quantitative Cell Science PART A

OMIP 073: Analysis of human thymocyte development with a 14-color flow cytometry panel

Sarah-Jolan Bremer[1] | Laura Glau[1] | Christina Gehbauer[1] | Annika Boxnick[1] | Daniel Biermann[2] | Jörg Siegmar Sachweh[2] | Eva Tolosa[1] | Anna Gieras[1]

[1]Department of Immunology, University Medical Center Hamburg-Eppendorf, Hamburg, Germany

[2]Surgery for Congenital Heart Disease, University Heart & Vascular Center Hamburg, University Medical Center Hamburg-Eppendorf, Hamburg, Germany

Correspondence
Anna Gieras, Universitätsklinikum Hamburg-Eppendorf, N27, Martinistraße 52, 20246 Hamburg, Germany.
Email: a.gieras@uke.de

Funding information
Deutsche Forschungsgemeinschaft, Grant/Award Number: KFO296; German Academic Scholarship Foundation; Werner Otto Stiftung

Abstract

This panel was designed for the identification and detailed characterization of the different developmental steps of human thymocytes. We optimized the panel for fresh tissue in order to provide an unbiased analysis of T cell development. Accurate selection of antibodies and precise gating allow us to phenotype 14 major stages of human thymocyte development and illustrate the trajectories of T cell development from early thymic progenitors (ETP) to mature T cells that are ready to populate the periphery. The panel identifies ETPs, T-lineage-committed cells (TC), CD34-positive immature single-positive CD4 cells (ISP4 CD34+), CD34-negative immature single-positive CD4 cells (ISP4 CD34-), CD45-low early double-positive cells (EDP CD45low), CD45-high early double-positive cells (EDP CD45high), late double-positive cells (LDP), single-positive CD4 cells (SP4), single-positive CD8 cells (SP8), ready-to-egress single-positive CD4 cells (rSP4), ready-to-egress single-positive CD8 cells (rSP8), T γδ cells (Tγδ), T regulatory cells (Treg), and ready-to-egress T regulatory cells (rTreg). To highlight important checkpoints during T cell development, we added antibodies relevant for specific developmental steps to the panel. These include CD1a to define TCs, CD28 as a marker for ß-selection and CD69 in combination with CD45RA to determine the maturation stage of thymocytes shortly before they become ready to egress the thymus and colonize the periphery. Moreover, Annexin V, as a marker for apoptosis, provides valuable extra information concerning the apoptotic death of thymocytes. Currently, we use this panel to identify aberrations in T cell development in health and disease.

KEYWORDS
apoptosis, flow cytometry, human, T cell development, thymocytes, thymus

1 | BACKGROUND

The thymus plays an essential role in establishing a functional adaptive immune system by providing the microenvironment for T cell development (1, 2). A detailed understanding of the developmental steps and cell populations in the human thymus will increase our knowledge about the origin of immune deficiencies, autoimmunity, or hematological diseases. Although T cell development has been characterized in depth in mice (3, 4), there is still some knowledge lacking concerning the development in humans, especially in the early stages

of development. Recently published investigations on single-cell RNA sequencing and CD marker expression of thymocytes give valuable information about the heterogeneity of thymocytes and their molecular landscape (5–9). To make research results on human T cell development comparable, a consensus should be found on classification and characteristics for human thymocyte populations. We aimed to design a panel (Table 1) that allows for easy and, at the same time, unmistakable definition of thymocyte subpopulations (Figure 1(A)), to give an overview of the developmental pathway (Figure 1(B)), and to provide reference values for the defined developmental stages (Figure 1(C)).

We first determined the live cell population using live/dead staining and Annexin V (for used antibodies see Table 2). By binding to phosphatidylserine, Annexin V detects not only necrotic, but also apoptotic cells (10). Since we have observed that thymocytes undergo apoptosis upon exposure to stressful stimuli like glucocorticoids or freezing, staining with Annexin V is a powerful tool to ensure the analysis of only live cells. The possibility of staining for Annexin V-binding makes our panel suitable for the determination of apoptotic thymocytes in in vitro assays.

CD34+ hematopoietic stem and progenitor cells migrate from the bone marrow to the thymus, where they undergo specialized processes of maturation and selection (11). These early thymic progenitors (ETP) can be defined as CD34+ CD45RA+ CD1a- and can give rise to different immune cell types. Upon Notch signaling, T cell-specific genes like *CD7* are upregulated (5, 12, 13). The progenitors are T-lineage-committed (TC) when they express CD1a, and the development of other lineages such as B cells, NK cells, or DCs is inhibited (1, 14). Rearrangement of the T cell receptor (TCR) takes place within a CD7+ subset, and at this stage, CD4 is upregulated and CD34 downregulated (15). Therefore, the immature single positive stage (ISP4) can be divided into a CD4+ CD34+ and a CD4+ CD34- population. Moreover, we discovered a population of early double-positive (EDP) cells expressing CD4 and CD8 that still express CD7, intermediate levels of CD34 and show low-level expression of CD45 (EDP CD45low). These findings indicate that ISP4 thymocytes do not necessarily completely lose CD34 expression or gain high levels of CD45 before becoming double-positive.

Expression of a functional TCR β chain that will pair with a pre-TCR α chain parallels development of progenitors into CD4+ CD8+ (double-positive) cells. TCR α rearrangement paves the way for a functional TCR αβ-CD3 complex that can be primarily seen in the double-positive population (1). The double-positive cells can be further subdivided into a CD4+ CD8+ CD3- (early double-positive [EDP]) and a CD4+ CD8+ CD3+ (late double-positive [LDP]) population. CD28 expression correlates with the expression of TCR β chain and provides information on ß-selection at different developmental stages (16). Rearrangement of the TCR γ and TCR δ loci occurs even before the TCR β chain is recombined, and thymocytes keep their γδ potential from the TC stage onwards for an elongated period (17). Cells with functionally rearranged TCR γ and TCR δ chains become CD3+ T γδ cells (18). Thymocytes undergo tightly regulated selection processes to gain a broad but self-tolerant TCR repertoire (19, 20). Thymocytes expressing a TCR that does not recognize self-MHC-peptides die by neglect, while thymocytes expressing a TCR with an excessive affinity for self-MHC-peptides are considered to be potentially autoreactive and undergo negative selection. Cells with a low to moderate affinity are positively selected (19). Positively selected thymocytes differentiate into CD8+ cytotoxic T cells or CD4+ helper T cells during selection processes, depending on their specificity of the clonal TCR to MHC class I or MHC class II molecules, respectively (21). Cells with a higher TCR signal strength are likely to become T regulatory cells (Treg) characterized by the expression of CD25 and FOXP3 (22). Recent findings suggest that Treg-commitment takes place already at the DP stage (23). In order to leave their thymic environment and migrate to the periphery, single-positive CD4 (SP4), single-positive CD8 (SP8), or Treg cells need to lose their retention marker CD69 and upregulate CD45RA (2). Finally, T cells that are ready to egress from the thymus can be identified by a CD3+ CD45RA+ CD69- phenotype.

The average percentages of the 14 subpopulations are depicted in Figure 1(C) (see also Online Table 7). DPs constitute the largest subpopulation with more than three-quarters of all thymocytes. Here, EDPs are more than twice the number of LDPs. The more immature (CD45low) compartment is dominated by ISP4 CD34+ cells. The largest subpopulation within the more mature (CD45high) compartment is SP4, followed by SP8, Treg and T γδ cells.

To visualize the co-expression of all markers on each cell simultaneously, we performed the dimensionality reduction algorithm UMAP (Uniform Manifold Approximation and Projection) (24) on the live, CD45+ cell population (Figure 1(D)). The UMAP overlay plot (Figure 1 (E)) shows all thymocyte subpopulations segregated according to the gating strategy (Figure 1(A)).

In summary, we use this 14-color panel to study the thymus of immunologically healthy children as well as children that display immunodeficiencies or have syndromes associated with immunological alterations. Since thymic tissue is taken from infants undergoing corrective cardiac surgery, this panel will be of special interest for researchers investigating the link between congenital heart diseases and alterations in the immune system.

TABLE 1 Summary table

Purpose	Comprehensive immunophenotyping of thymocytes
Species	Human
Cell types	Thymocytes
Cross-reference	None to date

2 | HUMAN SAMPLES

Thymic tissue was obtained from children up to the age of 3 years undergoing corrective cardiac surgery at the University Heart & Vascular Center Hamburg in 2018–2020. Patients with known syndromes (i.e., Down Syndrome, DiGeorge Syndrome) were excluded from

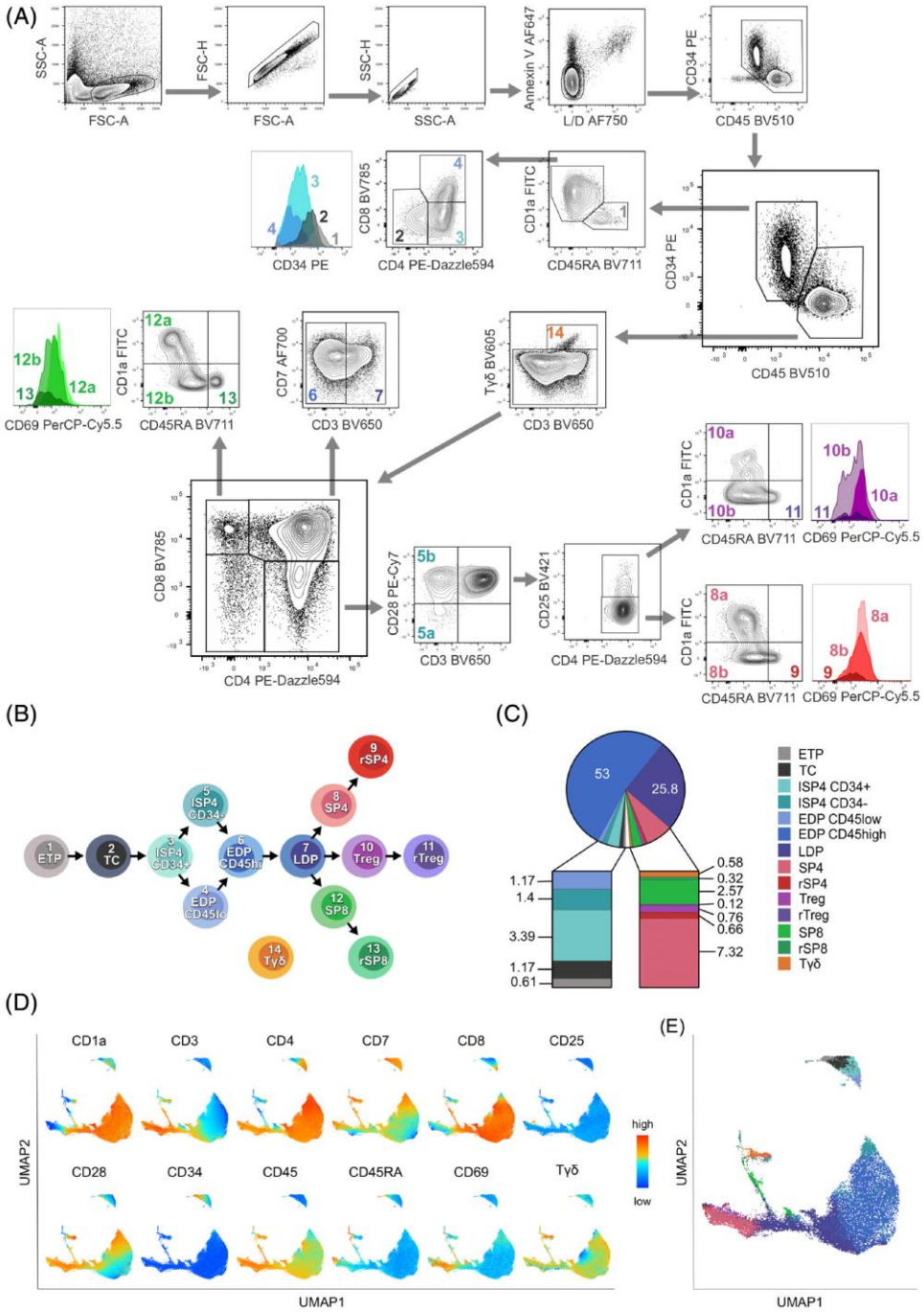

FIGURE 1 (A) Gating strategy for a 14-color flow cytometry panel to immunophenotype human thymocytes. The figure shows a representative sample of a 9-month-old donor. (B) T cell development in the human thymus. Developmental stages are numbered according to the gating in (A). (C) Average frequencies of human thymocyte subsets (percentage of CD45+ cells) in children aged 6–12 months. The insets show the least frequent subsets: left, subpopulations before EDP CD45high stage; right, subpopulations after LDP stage (n = 8). (D and E) UMAP analysis of 78,000 exported CD45+ cells. (D) UMAP plots visualizing the expression of each individual cell surface marker. (E) UMAP overlay plot illustrating all major thymocyte subpopulations. 1 ETP, early thymic progenitors; 2 TC, T-lineage-committed cells; 3 ISP4 CD34+, CD34-positive immature single-positive CD4 cells; 4 EDP CD45low, CD45-low CD34-positive early double-positive cells; 5 (5a+5b) ISP4 CD34-, CD34-negative immature single-positive CD4 cells; 6 EDP CD45high, CD45-high CD34-negative early double-positive cells; 7 LDP, late double-positive cells; 8 (8a+8b)SP4, CD4-single-positive cells; 9 rSP4, ready-to-egress CD4-single-positive cells; 10 (10a+10b) Treg, T regulatory cells; 11 rTreg, ready-to-egress T regulatory cells; 12 (12a+12b) SP8, CD8-single-positive cells; 13 rSP8, ready-to-egress CD8-single-positive cells; 14 T γδ, T γδ cells

TABLE 2 Reagents used for this OMIP

Antibody	Fluorochrome	Clone	Purpose
CD25	BV421	BC96	T regulatory cells
CD45	BV510	HI30	Leucocytes
Tγδ	BV605	11F2	T γδ cells
CD3	BV650	OKT3	T cells
CD45RA	BV711	HI100	Lineage marker during early and late developmental stages
CD8a	BV785	RPA-T8	CD8 T cells and double-positive cells
CD1a	FITC	HI149	T cell lineage commitment
CD69	PerCP-Cy5.5	FN50	Tissue retention marker
CD34	PE	563	Hematopoietic stem and progenitor cells
CD4	PE-Dazzle594	RPA-T4	CD4 T cells, ISP4 and double-positive cells
CD28	PE-Cy7	CD28.2	ß-selection
AnnexinV	AF647		Apoptosis
CD7	AF700	M-T701	T cell lineage
L/D	AF750		Viability

analysis. The study was approved by the local ethics committee and written informed consent was received from the parents (approved protocol number PV5482).

SIMILARITY TO OTHER OMIPs

None to date.

ACKNOWLEDGMENTS

We would like to thank the Flow Cytometry Core Facility of the University Medical Center Hamburg-Eppendorf for their support, instrument maintenance, and configuration. Special thanks go to Manuela Kolster, Romy Hackbusch, and Sabine Ahrendt for their help with tissue preparation, staining, and productive discussions. In addition, we want to thank Barbara Remberg and Michael Koch for organization. Finally, we are grateful to all our donors and their parents. This work was supported by the German Research Foundation (DFG, KFO296 to Eva Tolosa), the Werner Otto Foundation (Anna Giera), the German Academic Scholarship Foundation (Christina Gehbauer and Sarah-Jolan Bremer), and the graduate school program of the DFG (Sarah-Jolan Bremer). Open Access funding enabled and organized by Projekt DEAL.

AUTHOR CONTRIBUTIONS

Sarah-Jolan Bremer: Data curation; formal analysis; funding acquisition; investigation; project administration; validation; visualization; writing-original draft; writing-review & editing. **Laura Glau:** Formal analysis; software; visualization; writing-review & editing. **Christina Gehbauer:** Project administration; validation; writing-review & editing. **Annika Boxnick:** Data curation; validation; writing-review & editing. **Daniel Biermann:** Resources; validation; writing-review & editing. **Jörg Siegmar Sachweh:** Resources; validation; writing-review & editing. **Eva Tolosa:** Conceptualization; formal analysis; funding acquisition; methodology; project administration; resources; supervision; validation; visualization; writing-original draft; writing-review & editing. **Anna Gieras:** Conceptualization; data curation; formal analysis; funding acquisition; project administration; supervision; validation; visualization; writing-original draft; writing-review & editing.

CONFLICT OF INTERESTS

The authors have no conflicts of interest to declare.

ORCID

Anna Gieras https://orcid.org/0000-0002-5147-2281

REFERENCES

1. Spits H. Development of αβ T cells in the human thymus. Nat Rev Immunol. 2002;2(10):760–72.
2. Plum J, De Smedt M, Leclercq G, Taghon T, Kerre T, Vandekerckhove B. Human intrathymic development: A selective approach. Semin Immunopathol. 2008;30(4):411–23.
3. Zúñiga-Pflücker J. T-cell development made simple. Nat Rev Immunol. 2004;4(1):67–72.
4. Germain RN. T-cell development and the CD4–CD8 lineage decision. Nat Rev Immunol. 2002;2(5):309–22.
5. Lavaert M, Liang KL, Vandamme N, Park J-E, Roels J, Kowalczyk MS, et al. Integrated scRNA-Seq identifies human postnatal thymus seeding progenitors and regulatory dynamics of differentiating immature thymocytes. Immunity. 2020;52:1–17.
6. Park JE, Botting RA, Conde CD, Popescu DM, Lavaert M, Kunz DJ, et al. A cell atlas of human thymic development defines T cell repertoire formation. Science. 2020;367(6480):1–11.
7. Kalina T, Fišer K, Pérez-Andrés M, Kuˇzílková D, Cuenca M, SJW B, et al. CD maps–dynamic profiling of CD1–CD100 surface expression on human leukocyte and lymphocyte subsets. Front Immunol. 2019; 10(2434):1–15.
8. Zhou W, Yui MA, Williams BA, Yun J, Wold BJ, Cai L, et al. Single-cell analysis reveals regulatory gene expression dynamics leading to lineage commitment in early T cell development. Cell Syst. 2019;9(4): 321–37.
9. Chopp LB, Gopalan V, Ciucci T, Ruchinskas A, Rae Z, Lagarde M, et al. An integrated epigenomic and transcriptomic map of mouse and human αβ T cell development. Immunity. 2020;53(6):1182–201.

10. Crowley LC, Marfell BJ, Scott AP, Waterhouse NJ. Quantitation of apoptosis and necrosis by annexin v binding, propidium iodide uptake and flow cytometry. Cold Spring Harb Protoc. 2016;11:953–7.
11. Yoganathan K, Chen ELY, Singh J, Zúñiga-Pflücker JC. T-cell development: from T-lineage specification to Intrathymic maturation. In: Passos GA, editor. Thymus Transcriptome and cell biology. London: Springer-Nature; 2019. p. 67–115.
12. Schmitt TM, Zúñiga-Pflücker JC. Induction of T cell development from hematopoietic progenitor cells by delta-like-1 in vitro. Immunity. 2002;17(6):749–56.
13. Weerkamp F, Pike-Overzet K, Staal FJT. T-sing progenitors to commit. Trends Immunol. 2006;27(3):125–31.
14. Spits H, Blom B, Jaleco AC, Weijer K, Verschuren MCM, Van Dongen JJM, et al. Early stages in the development of human T, natural killer and thymic dendritic cells. Immunol Rev. 1998;165:75–86.
15. Van de Valle I, Davids K, Taghon T. Characterization and isolation of human T cell progenitors. In: Bosselut R, Vacchio MS, editors. T-cell development. Methods and protocols. Volume 1323. New York: Springer; 2016. p. 221–37.
16. Taghon T, Van de Walle I, De Smet G, De Smedt M, Leclercq G, Vandekerckhove B, et al. Notch signaling is required for proliferation but not for differentiation at a well-defined beta-selection checkpoint during human T-cell development. Blood. 2009;113(14):3254–63.
17. Dik WA, Pike-Overzet K, Weerkamp F, de Ridder D, de Haas EFE, Baert MRM, et al. New insights on human T cell development by quantitative T cell receptor gene rearrangement studies and gene expression profiling. J Exp Med. 2005;201(11):1715–23.
18. Taghon T, Rothenberg EV. Molecular mechanisms that control mouse and human TCR-αβ and TCR-γδ T cell development. Semin Immunopathol. 2008;30(4):383–98.
19. Klein L, Kyewski B, Allen PM, Hogquist KA. Positive and negative selection of the T cell repertoire: What thymocytes see (and don't see). Nat Rev Immunol. 2014;14(6):377–91.
20. Starr TK, Jameson SC, Positive HKA. Negative selection of T cells. Annu Rev Immunol. 2003;21(1):139–76.
21. Egawa T. Regulation of CD4 and CD8 coreceptor expression and CD4 versus CD8 lineage decisions. Adv Immunol. 2015;125(1):1–40.
22. Owen DL, Sjaastad LE, Farrar MA. Regulatory T cell development in the thymus. J Immunol. 2019;203(8):2031–41.
23. Vanhanen R, Leskinen K, Mattila IP, Saavalainen P, Arstila TP. Epigenetic and transcriptional analysis supports human regulatory T cell commitment at the CD4+CD8+ thymocyte stage. Cell Immunol. 2020;347:1–7.
24. McInnes L, Healy J, Melville J. UMAP: Uniform Manifold Approximation and Projection for Dimension Reduction. 2018. p. 1–51.Available from: http://arxiv.org/abs/1802.03426.

SUPPORTING INFORMATION

Additional supporting information may be found online in the Supporting Information section at the end of this article.

How to cite this article: Bremer S-J, Glau L, Gehbauer C, et al. OMIP 073: Analysis of human thymocyte development with a 14-color flow cytometry panel. *Cytometry*. 2021;1–5. https://doi.org/10.1002/cyto.a.24326

1.1 SUPPLEMENTARY MATERIAL

OMIP 073: Analysis of human thymocyte development with a 14-color flow cytometry panel

Sarah-Jolan Bremer, Laura Glau, Christina Gehbauer, Annika Boxnick, Daniel Biermann, Jörg Siegmar Sachweh, Eva Tolosa, Anna Gieras

ONLINE MATERIAL

Overall strategy for panel design

This 14-color thymocyte panel can be used to assess the frequencies or isolate the most relevant thymocyte subpopulations during human T cell development (Online Figure 1). We propose an easy-to-follow nomenclature and provide reference values for the different stages of human T cell development.

Identification of developing thymocytes

The gating strategy is shown in Figure 1A. We initially selected thymocytes on a FSC-A/SSC-A plot and removed doublets on FSC-A/FSC-H as well as SSC-A/SSC-H plots. We determined the live cell population using live/dead staining and Annexin V. Using only the live/dead staining, a significant fraction of apoptotic cells might remain undetected. Addition of Annexin V, which binds to phosphatidylserine present on the surface of apoptotic cells even at early stages (1), offers the opportunity to exclude (or include, if desired) apoptotic cells from the analysis. The next step was the exclusion of CD45- cells. CD45 is expressed on all mature leukocytes and is acquired early in development: Early precursors entering the thymus express intermediate levels of CD45 (CD45low) and acquire full expression later in development. CD45low thymocytes express CD34, a marker of hematopoietic stem and progenitor cells that is downregulated as cells undergo maturation (2). Using our panel, the earliest subpopulation to detect are early thymic progenitors (ETP **(1)**), with a

CD45RA+ (2) and CD1a- (3) phenotype. The expression of CD1a marks T-lineage-commitment in human thymocytes (4,5). It has been recently shown that the loss of CD44 occurs slightly prior to the upregulation of CD1a (6), therefore, CD44 could alternatively be used as a marker for T-lineage-commitment. Within CD1a+ immature (CD45low CD34+) cells, we distinguish three populations: CD7+ CD4- CD8- T-lineage-committed cells (TC **(2)**), CD3- CD4+ CD8- immature single-positive cells (ISP4 CD34+ **(3)**) (7) and, interestingly, also cells that are early double-positive CD3- CD4+ CD8+ (EDP CD45low **(4)**). The discovery of early double-positive cells within the CD45low CD34+ population was surprising, since double-positive cells were only known to develop out of CD34- ISP4 cells (5). Our analysis of differentiating thymocytes shows a small but consistent population of cells that acquires CD8 before completely losing CD34 and before upregulation of CD45 surface expression. This population has not been described previously, and functional studies will be necessary to determine its exact maturation stage and functional relevance.

We next analyzed the compartment of cells expressing high levels of CD45 and lacking CD34, indicating more mature thymocytes. For this, we first excluded T cells of the T γδ lineage (T γδ cells **(14)**). Even though the vast majority of early thymocytes will develop into T cells harboring a TCR αβ receptor, a small proportion (ca 0.1-1% (8)) develops into TCR γδ cells, which in the thymus may or may not express the co-receptors CD4 and CD8. Since the developmental pathway and markers for human T γδ cells are all but clear (9), we decided to exclude them from further analysis, in order to avoid having mature T γδ cells in the double-negative compartment. The remaining T γδ- CD34- CD45high cells were plotted in the CD4 vs CD8 graph. Here, four populations could be detected: the highly abundant double-positive CD4+ CD8+ thymocytes, cells expressing either CD4 or CD8 co-receptors, and a small population of cells in the lower left quadrant. This small cell population contains a mixture of non-T cell precursors, namely B cells, NK cells (Online Figure 2), and other innate lymphoid subpopulations, mainly DCs, in minute numbers, as shown by single-cell RNA sequencing of the human thymus (6, 10, 11). The lower right compartment of cells expressing CD4 but not CD8 contains two major subpopulations. The population that does not express CD3 is the

most immature subpopulation within the CD34- CD45high compartment, and is named ISP4 CD34- **(5)** (2). This cell population can be further divided according to the expression of CD28 **(5a, 5b),** which in thymocytes is a marker for cells that have passed the ß-selection checkpoint (12). Importantly, the absence of CD28 in some ISP4 thymocytes shows that - in contrast to mouse ISP cells - not the entire human ISP4 cell population has passed the ß-selection checkpoint yet (7). Looking at the next developmental step, the double-positive (DP) cells, we can distinguish CD3- early double-positive cells (EDP CD45high **(6)**) and CD3+ late double-positive cells (LDP **(7)**). They do not appear as two clearly distinct populations, most probably because development does not take place in discrete steps, but rather in a continuum. Interestingly, DP cells display a heterogeneous expression pattern of CD7, which does not correlate with the levels of CD3-expression. *CD7* is a Notch target gene as *CD3E* and mainly analyzed in the immature subpopulations as a marker for Notch activation (6). Further studies are required concerning CD7 expression in the more mature populations. Depending on selection events and MHC binding, DP cells develop either into CD4+ **(8)** or CD8+ **(12)** single-positive cells (reviewed in (13)). CD4+ CD3+ cells are now all positive for CD28, i.e. after ß-selection. Within the SP4 population, T regulatory cells (Treg **(10)**) can be identified by the expression of CD25. CD8 SP cells are the ones appearing in the upper left quadrant of the CD4/CD8 plot. The CD4 SP, CD8 SP, and Treg subpopulations can be divided according to the expression of CD1a. We could further identify the cells that are ready to egress from the thymus (rSP4 **(9)**, rTreg **(11)**, rSP8 **(13)**) (5,14). These cells have lost the expression of CD69 (a tissue retention marker (14,15)) (Online Figure 3) as well as CD1a, and express high levels of CD45RA, having now reached the phenotype of naïve T cells in the periphery.

Panel development and optimization

The OMIP was developed for a 4-laser BD LSR Fortessa with a 405 nm violet laser with 7 PMTs (photomultiplier tubes), a 488 nm blue laser with 3 PMTs, a 561 nm yellow/green laser with 5 PMTs and a red laser with 3 PMTs (for information on long pass (LP) filter and band pass (BP) filter see Online Table 1). Since one detector is used for SSC, the instrument can detect up to 17 dyes in one

sample. We set up a 14-color panel to work comfortably on the cytometer (Online Table 2). Additionally, BV570 could be used if exclusion of other population markers (i.e. B or NK cells) is desired. Quality control of the cytometer is regularly performed at our core facility as well as standardized procedures for starting, cleaning and shutting down the instrument.

During our panel optimization process, we tested three different thymocyte panels (Online Figure 1, Online Table 3) on two different BD flow cytometry instruments. The final OMIP is a combination of panel I and II – initially designed for a 3-laser BD Celesta - and includes the most important markers for human T cell development with an optimal combination of antibody clones and fluorochromes to ensure good sensitivity. The advantage of the final OMIP is the possibility to analyze all defined thymocyte subpopulations in one tube, whereas panel I and II can only be used to dissect either the more immature (early development) or the more mature subpopulations (late development), respectively (Online Figure 4). The possibility to study all subpopulations with one panel improves statistical analysis and allows visualization of the multi-dimensional data at all developmental stages (Figure 1D vs. Online Figure 4).

To make the panel widely applicable, we only used commercially available antibodies. We followed the principle of using bright fluorochromes to detect weakly expressed surface markers (CD25-BV421, CD34-PE, CD45RA-BV711) and vice versa (CD1a-FITC, CD3-BV650, CD7-AF700, CD8a-BV785, CD45-BV510). In order to improve separation of populations and to reduce spectral overlap, we placed markers that are important for defining populations according to our gating strategy on different lasers. As an example, to distinguish early precursors from more mature thymocyte populations, we plotted CD34 against CD45. CD45 is measured using the violet laser (BV510), while CD34 is measured using the yellow/green laser (PE). In panel I, we used the combination of CD45-BV510 (clone HI30) and CD34-BV650 (clone 561). Due to low separation, we tested a variety of clones as well as fluorochrome combinations and finally kept CD45-BV510 (clone HI30) but switched to CD34-PE (clone 563) which then allowed optimal gating of the CD45low CD34+ population (Online Table 4, Online Figure 5). In order to distinguish the main more mature thymic populations, the

intensity of staining for CD4 and CD8 needs to be high. For this reason, we used a relatively bright fluorochrome for CD4 (PE-Dazzle594) on the yellow/green laser and a less bright fluorochrome (BV785) on the violet laser for CD8 in our final OMIP. These two markers are crucial for the phenotypic analysis of thymocytes. Therefore, it is absolutely necessary to find the best reagents to enable an ideal separation of CD4+ cells, CD8+ cells and the most abundant thymocyte subpopulation, the DP cells. For CD4, we tested CD4-BV421 (clone RPA-T4) which showed good separation and CD4-AF700 (clone OKT4) which showed insufficient separation in panel I and II, respectively. Extensive optimization was performed by using a selection of anti-CD4 and anti-CD8 antibodies (Online Table 4). CD4-PE-Dazzle594 (clone RPA-T4) turned out to be optimal. For CD8, CD8-BV785 (clone RPA-T8) proofed better separation than CD8-BV605 (clone RPA-T8) in panel II or other tested combinations. Another important but rare cell type are T regulatory cells which are defined by co-expression of CD4 and CD25. After optimization of different anti-CD4 and anti-CD8 reagents, CD4 was placed on the yellow/green laser. Therefore, we placed CD25 on the violet laser (BV421) for optimal separation. CD45RA was assigned to the bright fluorochrome BV711 because of its low expression. Before changing to the BD LSR-Fortessa we tested a slightly dimmer reagent - CD45RA-BV785 - and this showed good separation, too. In our OMIP we used T γδ-BV605 (clone 11F2) for the detection of T γδ cells. Alternatively, T γδ-PE-Cy7 could be used, since it showed good separation, too. Even if the staining for T γδ cells was not very bright, gating of T γδ cells was still easily possible. Correct percentages of positive cells were confirmed by comparing the percentages of T γδ cells obtained with this panel to the percentages obtained in a separate 12-color T γδ panel (not shown). Of note, we chose clone OKT3 for CD3 because it does not interfere with staining of T γδ cells using clone 11F2. In previous experiments we had found clone 11F2 to be superior to clone B1 (Online Figure 6). Clone 11F2, which recognizes a framework epitope of the T cell γδ receptor, was chosen to mark all T γδ cells. All clones used for this panel are commercially available standard clones.

CD38 was used in the original panel I (early development). It is upregulated when hematopoietic stem cells (CD34+ CD38-) become lymphoid (CD34+ CD38+ CD45RA+), myeloid (CD34+ CD38+ CD45RA+) or erythroid (CD34+ CD38+ CD45RA-) progenitors (3, 16). A diminutive population of CD34+ CD38- CD1a- cells can be found in the thymus (17) and is detectable with panel I (Online Figure 7A). All other thymocytes express CD38 at high levels (Online Figure 4A) (18). Within the CD38+ compartment of the ETPs, CD7 is upregulated upon Notch-signaling, followed by CD5, even before the cells become T-lineage-committed (CD1a+) (19). Both progenitors, CD34+ CD7- and CD34+ CD7int cells, can differentiate into CD7+ CD1a+ T-lineage-committed thymocytes (9). In panel I, we tested CD5-PerCP-Cy5.5 and CD7-AF700 to identify CD34+ CD1a- CD7- cells, CD34+ CD1a- CD7+ cells and within this population CD5- as well as CD5+ subsets (3). CD7 showed better separation than CD5 (Online Figure 7B). We detected a tiny population of CD7- CD5+ cells which could either have gained CD5 before CD7 upon Notch-signaling or could represent CD5+ innate lymphoid cells (20). For the final OMIP we decided to include CD1a as a well characterized marker for T cell lineage commitment as well as CD7 as a marker for Notch-signaling.

All antibodies that were tested during panel optimization but excluded in the final OMIP are shown in Online Table 4.

Antibody titrations, PMT voltages and compensation matrix

Before panel design and in order to find the best fluorochrome combinations for our instrument, we produced a spillover spreading matrix (SSM) (21) using single-stained controls for all available detectors. Rarely expressed markers were placed in channels with minimal loss of resolution.

In order to reduce unspecific binding and ensure optimal sensitivity during flow cytometry measurement, we optimized the concentration of antibodies used for our specific specimen (human thymocytes) and for the instrument (BD LSR Fortessa). Therefore, we performed titrations of all fluorochrome-conjugated antibodies in 1:3 dilution steps on human thymocytes (Online Figure 8). Antibodies for surface markers with low expression (CD25, CD69, T γδ) where titrated in

147 combination with anti-CD3 fluorochrome-conjugated antibodies (and anti-CD4 for titration of CD25-
148 BV421). The separation index was calculated in order to select the optimal reagent titers using the
149 formula

150 $$Separation\ Index = \frac{Median\ Positive - Median\ Negative}{(84th\ Percentile\ Negative - Median\ Negative) \div 0.995} \quad (22).$$

151 The PMT voltages were optimized at the beginning of panel development to ensure the detection of
152 all populations and checked for each experiment to ensure that all cell subpopulations are within
153 scale.

154 A compensation matrix was calculated using fresh thymocytes stained with each single
155 fluorochrome-labelled antibody. For an accurate determination of the compensation matrix, we
156 used the same antibodies that are used in the panel for bright/abundant markers and alternative
157 reagents for makers with low expression levels (CD69) or low frequency populations (Tγδ, CD25,
158 CD45RA), where we used anti-CD4-antibodies conjugated to the respective fluorochrome (see
159 Online Table 5). This alternative approach was chosen for the following reasons: First, since
160 fluorochromes can show different spectral characteristics when coupled to cells or beads (23), we
161 routinely consider to perform compensation experiments with the cells of interest. Second, the use
162 of alternative antibodies guarantees a high number of positive events and provides a strong signal.
163 Finally, we did not experience any compensation problems when establishing the panel, so we kept
164 the alternative approach with the use of cells and alternative antibodies for CD25, CD45RA, CD69
165 and Tγδ for the analysis of human thymocytes. However, it is important to consider that the use of
166 alternative antibodies conjugated to tandem dyes (in that case Tγδ-BV605, CD45RA-BV711 and
167 CD69-PerCP-Cy5.5) can lead to an inappropriate compensation matrix since the dye-to-dye ratios
168 may differ between lots and this may lead to differences in the emission spectra. Therefore, each lot
169 needs to be considered as a different reagent (24). To confirm that the use of alternative antibodies
170 coupled to tandem dyes (listed in Online Table 5) did not result in inaccurate compensation for our
171 panel, we compared the compensation matrices obtained with the two approaches in a NxN plot of

172 single cells in FlowJo. The pattern of the two matrices is similar even though the values are not
173 identical (Online Table 6). Importantly, the NxN plots show that we obtained a proper compensation
174 using both strategies (Online Figure 9) and the discrimination of thymocyte subpopulations was not
175 affected by the compensation approach used. As previously stated by Liechti and Roederer (23), we
176 recommend to compare cell- and bead-based compensation controls during the establishment of
177 the panel. When different reagents, including different lots, than those listed in Online Table 5 are
178 used as alternative antibodies, the compensation matrix will differ and might not provide adequate
179 compensation values. In this case, the use of beads and the exact same antibodies as in the panel
180 (Online Table 2) should be prioritized. For the compensation of Annexin V and live/dead staining for
181 the discrimination of dead cells, we used cell-based compensation controls. For this, we treated
182 thymocytes for 5 minutes at 65°C in order to induce cell death, mixed them 1:1 with untreated
183 thymocytes and distributed the cells equally in two tubes for unstained and stained compensation
184 controls.

185 **Quality control of flow cytometry data**

186 Flow cytometry data were subjected to quality control using the FlowJo plugin FlowAI
187 (https://pubmed.ncbi.nlm.nih.gov/27153628/). This algorithm automatically scans flow rate
188 (number of cells per unit of time), signal acquisition (stability of the signal over time) and dynamic
189 range (margin events of lower and upper limit) to identify and remove anomalous events from the
190 final analysis (25). We used default settings for the quality control of signal acquisition and dynamic
191 range on our entire dataset. After running FlowAI, two gates 'FlowAIGoodEvents' and
192 'FlowAIBadEvents' are generated and downstream analysis can be continued with cleaned data.

193 **Cryopreservation of human thymic tissue samples**

194 Human thymic tissue is not often available, and the use of cryopreserved samples would be highly
195 convenient. Unfortunately, thymocytes are extremely sensitive to cryopreservation/thawing, and
196 many cells die, leading to a strong bias in the distribution of different thymocyte populations. We

compared the frequencies of subpopulations in fresh and thawed thymocytes after freezing at -80°C or in liquid nitrogen as part of our protocol optimization. Additionally, we tested two different cryopreservation protocols: cryopreservation protocol 1 with freezing medium containing 65% RPMI, 25% FBS and 10 % DMSO and cryopreservation protocol 2 with freezing medium containing 90% FBS and 10% DMSO (see materials and methods). Our results demonstrate considerable differences in the frequencies of thymocyte subpopulations after thawing, and show that high serum content in the freezing medium partially protects double-positive thymocytes from death (Online Figure 10). Based on these results, we always processed, stained and analyzed the thymic tissue within 6 hours after corrective heart surgery. We therefore strongly recommend using exclusively fresh tissue to obtain reliable and unbiased information on the composition of the major thymocyte subpopulations. If cryopreservation is unavoidable, the freezing medium should contain 90% FBS.

UMAP

During recent years, the technique of flow cytometry has developed quickly, leading to a raising number of parameters measured simultaneously. This increasing dimensionality of data acquired at one flow cytometer and the concomitant increase in time consumed by manual gating led to a collection of new analysis techniques for multi-dimensional data. One relatively new algorithm for dimensionality reduction, Uniform Manifold Approximation and Projection (UMAP), has become the gold standard for the representation and analysis of single-cell data besides t-distributed stochastic neighbor embedding (t-SNE) (26,27). By using a dimensionality reduction algorithm, it is possible to explore the co-expression of all markers on each cell simultaneously.

UMAP was run on roughly 78.000 pre-gated live CD45+ cells (including CD45high and CD45low cells) from one representative thymus sample using all remaining 12 fluorescence parameters as input for the algorithm (Figure 1D). The color-coding of the UMAP plot by intensity of marker expression was conducted for each marker individually to ensure the best color separation for each channel, ranging from blue (no expression) to red (high expression). We also created an UMAP overlay plot showing

the color-coded thymocyte subpopulations (Figure 1E). For average frequencies of thymocyte subsets see Online Table 7.

Additionally, we downsampled the selected live CD45+ cells to 5000 events and ran UMAP to see whether the main thymocyte subpopulations can still be analyzed. Online Figure 11 shows that all 14 subpopulations can be found in the downsampled UMAP overlay plot. This might be especially useful when using our 14-color panel for integrated proteomic and transcriptomic analysis (see next paragraph), where the number of cells analyzed is highly limited in contrast to flow cytometry.

Enhancing integrated analysis of proteomic and transcriptomic data

This panel was designed to characterize and/or sort different developmental stages of human thymocytes by flow cytometry. Additionally, the panel could facilitate the combination of proteomic and transcriptomic data analysis by using CITE-seq (cellular indexing of transcriptomes and epitopes by sequencing). CITE-seq allows the simultaneous measurement of protein markers with an unbiased transcriptome profiling of highly heterogeneous cell populations (28).

Sample variability and analysis

The median fluorescence intensity (MFI) for each marker may vary across different samples due to technical or sample variability, even after careful standardization of sample preparation and staining procedures. For traditional cell population gating during manual analysis of compensated fcs files, we relied on visual assessment of cell clusters in two dimensional plots to circumvent technical and biological differences among samples. For visualization and unbiased analysis of high dimensional flow cytometry data (e.g. using UMAP (26)) of merged fcs files from different samples we include a pre-processing step that normalizes MFI across samples (e.g the per-channel normalization method gaussNorm from the R package flowStats (29)).

References

1. Crowley LC, Marfell BJ, Scott AP, Waterhouse NJ. Quantitation of Apoptosis and Necrosis by Annexin V Binding, Propidium Iodide Uptake, and Flow Cytometry. Cold Spring Harb Protoc. 2016;11:953–7.

2. Spits H, Blom B, Jaleco AC, Weijer K, Verschuren MCM, Van Dongen JJM, et al. Early stages in the development of human T, natural killer and thymic dendritic cells. Immunol Rev. 1998;165:75–86.

3. Seet CS, He C, Bethune MT, Li S, Chick B, Gschweng EH, et al. Generation of mature T cells from human hematopoietic stem and progenitor cells in artificial thymic organoids. Nat Methods. 2017;14(5):521–30.

4. Weerkamp F, Baert MRM, Brugman MH, Dik WA, De Haas EFE, Visser TP, et al. Human thymus contains multipotent progenitors with T/B lymphoid, myeloid, and erythroid lineage potential. Blood. 2006;107(8):3131–7.

5. Plum J, De Smedt M, Leclercq G, Taghon T, Kerre T, Vandekerckhove B. Human intrathymic development: A selective approach. Semin Immunopathol. 2008;30(4):411–23.

6. Lavaert M, Liang KL, Vandamme N, Park J-E, Roels J, Kowalczyk MS, et al. Integrated scRNA-Seq Identifies Human Postnatal Thymus Seeding Progenitors and Regulatory Dynamics of Differentiating Immature Thymocytes. Immunity. 2020;52:1–17.

7. Valle I Van de, Davids K, Taghon T. Characterization and Isolation of Human T Cell Progenitors. In: Bosselut R, Vacchio MS, editors. T-Cell Development: Methods and Protocols. Vol.1323. New York: Springer; 2016. p. 221–37.

8. Borst J, van Dongen JJM, Bolhuis RLH, Peters PJ, Hafler DA, de Vries E, et al. Distinct Molecular Forms of Human T Cell Receptor g/d Detected on Viable T Cells by a Monoclonal Antibody. J Exp Med. 1988;167(5):1625–44.

9. Joachims ML, Chain JL, Hooker SW, Knott-Craig CJ, Thompson LF. Human αβ and γδ Thymocyte Development: TCR Gene Rearrangements, Intracellular TCRβ Expression, and γδ Developmental Potential--Differences between Men and Mice. J Immunol. 2006;176(3):1543–52.

10. Park JE, Botting RA, Conde CD, Popescu DM, Lavaert M, Kunz DJ, et al. A cell atlas of human thymic development defines T cell repertoire formation. Science. 2020;367(6480):1–11.

11. Weerkamp F, De Haas EFE, Naber BAE, Comans-Bitter WM, Bogers AJJC, Van Dongen JJM, et al. Age-related changes in the cellular composition of the thymus in children. J Allergy Clin Immunol. 2005;115(4):834–40.

12. Taghon T, Van de Walle I, De Smet G, De Smedt M, Leclercq G, Vandekerckhove B, et al. Notch signaling is required for proliferation but not for differentiation at a well-defined beta-selection checkpoint during human T-cell development. Blood. 2009;113(14):3254–63.

13. Germain RN. T-cell development and the CD4–CD8 lineage decision. Nat Rev Immunol. 2002;2(5):309–22.

14. Vanhecke D, Leclercq G, Plum J, Vandekerckhove B. Characterization of distinct stages during the differentiation of human CD69+CD3+ thymocytes and identification of thymic emigrants. J Immunol. 1995;155(4):1862–72.

15. Feng C, Woodside KJ, Vance BA, El-Khoury D, Canelles M, Lee J, et al. A potential role for CD69 in thymocyte emigration. Int Immunol. 2002;14(6):535–44.

16. Dircio-Maldonado R, Flores-Guzman P, Corral-Navarro J, Mondragón-García I, Hidalgo-Miranda A, Beltran-Anaya FO, et al. Functional Integrity and Gene Expression Profiles of Human Cord Blood-Derived Hematopoietic Stem and Progenitor Cells Generated In Vitro. Stem Cells Transl Med. 2018;7(8):602–14.

17. Dik WA, Pike-Overzet K, Weerkamp F, de Ridder D, de Haas EFE, Baert MRM, et al. New

insights on human T cell development by quantitative T cell receptor gene rearrangement studies and gene expression profiling. J Exp Med. 2005;201(11):1715–23.

18. Kalina T, Fišer K, Pérez-Andrés M, Kuˇzílková D, Cuenca M, Bartol SJW, et al. CD Maps — Dynamic Profiling of CD1 – CD100 Surface Expression on Human Leukocyte and Lymphocyte Subsets. Front Immunol. 2019;10(2434):1–15.

19. Brauer PM, Singh J, Xhiku S, Zúñiga-Pflücker JC. T Cell Genesis: In Vitro Veritas Est? Trends Immunol. 2016;37(12):889–901.

20. Nagasawa M, Germar K, Blom B, Spits H. Human CD5+ Innate Lymphoid Cells Are Functionally Immature and Their Development from CD34+ Progenitor Cells Is Regulated by Id2. Front Immunol. 2017;8(1047):1–12.

21. Nguyen R, Perfetto S, Mahnke YD, Chattopadhyay P, Roederer M. Quantifying Spillover Spreading for Comparing Instrument Performance and Aiding in Multicolor Panel Design. Cytom Part A. 2013;83 A(3):306–15.

22. Telford WG, Babin SA, Khorev SV, Rowe SH. Green Fiber Lasers: An Alternative to Traditional DPSS Green Lasers for Flow Cytometry. Cytom Part A. 2009;75A(12):1031–39.

23. Liechti T, Roederer M. OMIP-060: 30-Parameter Flow Cytometry Panel to Assess T Cell Effector Functions and Regulatory T Cells. Cytom Part A. 2019;95A(11):1129-34.

24. Johansson U, Macey M. Tandem Dyes: Stability in Cocktails and Compensation Considerations. Cytometry B Clin Cytom. 2014;86B(3):164-74.

25. Monaco G, Chen H, Poidinger M, Chen J, De Magalhães JP, Larbi A. FlowAI: Automatic and interactive anomaly discerning tools for flow cytometry data. Bioinformatics. 2016;32(16):2473–80.

26. McInnes L, Healy J, Melville J. UMAP: Uniform Manifold Approximation and Projection for Dimension Reduction. 2018. p. 1–51. Available from: http://arxiv.org/abs/1802.03426

316 27. van der Maaten L, Hinton G. Visualizing Data using t-SNE. J Mach Learn Res. 2008;9:2579–
317 605.

318 28. Stoeckius M, Hafemeister C, Stephenson W, Houck-loomis B, Chattopadhyay PK, Swerdlow H,
319 et al. Large-scale simultaneous measurement of epitopes and transcriptomes in single cells.
320 Nat Methods. 2017;14(9):865–8.

321 29. Florian Hahne, Nishant Gopalakrishnan, Alireza Hadj Khodabakhshi, Chao-Jen Wong and
322 Kyongryun Lee (2019). flowStats: Statistical methods for the analysis of flow cytometry data.
323 R package version 3.44.0. http://www.github.com/RGLab/flowStats

MATERIALS AND METHODS

Thymocyte single cell preparation and staining protocol

After resection of the thymus, the biological material was kept in DPBS and processed and analyzed with flow cytometry within six hours. Single-cell suspensions were prepared by mechanical disruption - without enzymatic digestion - and subsequent filtering through a 70 µm nylon mesh. Cells were washed with 1x Annexin V Binding Buffer and stained with following fluorochrome-conjugated antibodies: anti-CD1a FITC (clone: HI149), anti-CD3 BV650 (clone: OKT3), anti-CD4 PE-Dazzle594 (clone: RPA-T4), anti-CD7 AF700 (clone: M-T701), anti-CD8a BV785 (clone: RPA-T8), anti-CD25 BV421 (clone: BC96), anti-CD28 PE-Cy7 (CD28.2), anti-CD34 PE (clone: 563), anti-CD45 BV510 (clone: HI30), anti-CD45RA BV711 (clone: HI100), anti-CD69 PerCP-Cy5.5 (clone: FN50), anti-T γδ BV605 (clone: 11F2), Annexin V AF647, live/dead AF750.

Flow cytometry was performed on an LSR Fortessa (FACS LSRFortessa, Becton Dickinson, Franklin Lakes (NJ), USA). For information on reagents and materials see Online Table 8 and Online Table 9.

For used abbreviations see Online Table 10.

Self-made buffers and media:

Annexin-buffer (10x): H_2O with 1.4 M NaCl, 25 mM $CaCl_2$, 0.1 M HEPES

Flow buffer: PBS with 0.1 % BSA, 0.02 % NaN_3

Freezing medium I: RPMI with 10 % FBS (heat inactivated)

Freezing medium II: RPMI with 40 % FBS (heat inactivated), 20 % DMSO

Freezing medium III: 100% FBS (heat inactivated)

Freezing medium IV: 80% FBS (heat inactivated), 20 % DMSO

Isolation of thymocytes:

1. Collect thymic tissue from children undergoing corrective cardiac surgery.
2. Place thymic tissue in DPBS.
3. Sample is transferred to the lab (on ice).
4. Remove burned tissue mechanically (place tissue in petri dish on ice).
5. Cut thymus into little pieces.
6. Mesh thymus with the plunger of a syringe into a 50 ml tube (on ice) through a 70 µm cell strainer. Use x-vivo 15 (4°C) to rinse the cell strainer.
7. Centrifuge cells (450 × *g*, 4°C, 5 min).
8. Discard supernatant and resuspend cells in 20 ml x-vivo 15 (4°C).
9. Filter suspension again through a 70 µm cell strainer.
10. Count cells on chamber slides using trypan blue.

Surface staining protocol:

11. Transfer 1 million cells to each FACS tube ("panel" and "unstained").
12. Prepare antibody cocktail for 1 million cells (without adding Annexin V). Place antibody tubes on ice.
13. Fill antibody cocktail up to a total volume of 50 µl with Annexin buffer (1x).
14. Centrifuge FACS tubes with cells (450 × *g*, RT, 5 min) and discard supernatant.
15. Add 50 µl antibody cocktail and 5 µl Annexin V to FACS tube "panel".
16. Add 55 µl Annexin buffer to FACS tube "unstained".
17. Vortex tubes.
18. Incubate for 10 min at room temperature (RT), protect from light.
19. Prepare live/dead staining: add 1µl LIVE/DEAD dye to 250 µl PBS.

20. Add 50 µl of this suspension to the stained tube.
21. Vortex.
22. Incubate for 20 min at RT, in the dark.
23. Wash the cells by adding 1 ml Annexin buffer.
24. Vortex.
25. Centrifuge (450 × *g*, RT, 5 min).
26. Resuspend cells in 250 µl buffer for flow cytometry.
27. Analyze the cells on LSR Fortessa.

Cryopreservation protocol 1:

After isolation of thymocytes:

1. Use 500 million cells for 10 cryotubes.
2. Centrifuge (450 × *g*, 4°C, 5 min).
3. Discard supernatant and resuspend pellet in 5 ml freezing medium I (4°C).
4. Transfer 500 µl cell suspension to each cryotube on cooling rack or ice.
5. 10x: every 30 sec add 50 µl freezing medium II (4°C) and carefully swirl tube.
6. You have a final volume of 1 ml in each cryotube.
7. Place cryotubes in Mr. Frosty (Mr. Frosty™ Freezing container, Thermo Fisher Scientific, Waltham (MA), USA) and put Mr. Frosty in the freezer (-80°C). Should cool down slowly, ideally 1°C/min.
8. For long-term storage store samples in liquid nitrogen.

Cryopreservation protocol 2:

After isolation of thymocytes:

1. Use 500 million cells for 10 cryotubes.

2. Centrifuge (450 × *g*, 4°C, 5 min).
3. Discard supernatant and resuspend pellet in 5 ml freezing medium III (4°C).
4. Transfer 500 µl cell suspension to each cryotube on cooling rack or ice.
5. 10x: every 30 sec add 50 µl freezing medium IV (4°C) and carefully swirl tube.
6. You have a final volume of 1 ml in each cryotube.
7. Place cryotubes in Mr. Frosty (Mr. Frosty™ Freezing container, Thermo Fisher Scientific, Waltham (MA), USA) and put Mr. Frosty in the freezer (-80°C). Should cool down slowly, ideally 1°C/min.
8. For long-term storage store samples in liquid nitrogen.

Thawing of thymocytes:

1. Thaw cryotube with thymocytes in the water bath (37°C) until nearly ice-less.
2. Slowly add 1 ml RPMI (4°C) into cryotube.
3. Transfer cells into a 15 ml falcon tube with 5 ml RPMI (4°C).
4. Centrifuge (450 × *g*, 4°C, 5 min).
5. Discard supernatant and resuspend pellet in 5 ml RPMI + 50 µl DNase (c=10 mg/ml).
6. Incubate for 5 min at RT.
7. Filter suspension through a 70 µm cell strainer.
8. Centrifuge (450 × *g*, RT, 5 min).
9. Discard supernatant and add 1 ml x-vivo 15.
10. Centrifuge (450 × *g*, RT, 5 min).
11. Discard supernatant and add 1 ml x-vivo 15.

Data analysis

Flow cytometry data were analyzed using FlowJo 10.6.2 software (FlowJo, LLC, Ashland, USA). Statistical analysis was performed using GraphPad Prism 6.07 (GraphPad Software, Inc., La Jolla, USA). INKSCAPE (https://inkscape.org/de/) was used for figure production. UMAP analysis was performed in R using the R package flowCore for handling of FCS files. The dimensionality reduction of the compensated and transformed data was calculated using the R package umap with default parameters. The graphical representation was created using the R package ggplot2.

Software packages:

- R Core Team, *R: A language and environment for statistical computing.* 2019, R Foundation for Statistical Computing, Vienna, Austria
- Monaco G, Chen H. *flowAI: automatic and interactive quality control for flow cytometry data*. R package version 1.18.0. 2020
- B. Ellis, P.H., Florian Hahne, Nathan Le Meur, Nishat Gopalakrishnan, Josef Spidlen, Mike Jiang and Greg Finak, *flowCore: Basic structures for flow cytometry data.* 2019
- Konopka, T., *umap:Uniform Manifold Approximation and Projection.* 2019
- Wickham, H., *ggplot2: Elegant Graphics for Data Analysis.* 2016 Springer Verlag New York

ONLINE FIGURES AND ONLINE TABLES

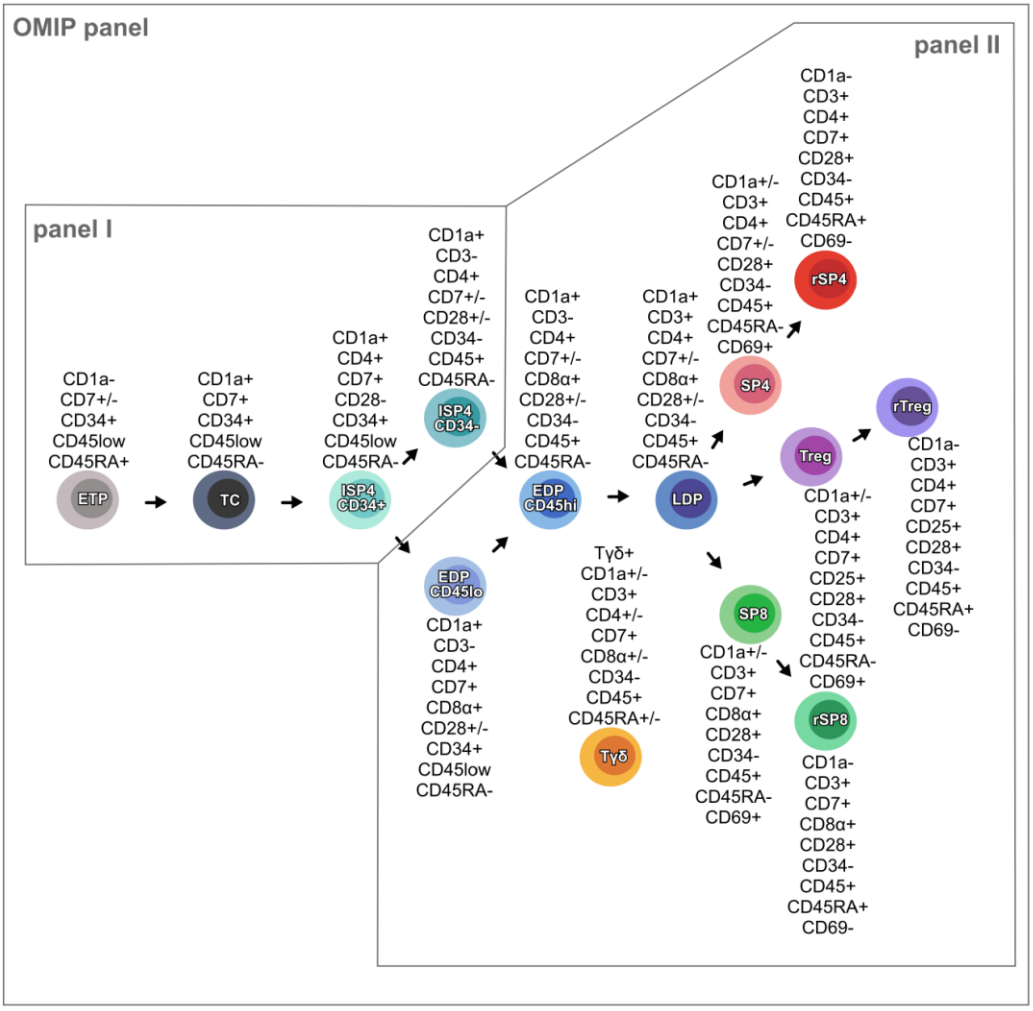

Online Figure 1. T cell development in the human thymus. The figure shows the developmental stages with expressed surface markers. Panel I was developed to analyze more immature thymocytes, panel II to analyze more mature thymocytes. The OMIP is the combination of panel I and II (cells detected with the respective panel are framed). Abbreviations: ETP: early thymic progenitors, TC: T-lineage-committed cells, ISP4 CD34+: CD34-positive immature single-positive CD4 cells, EDP CD45low: CD45-low CD34-positive early double-positive cells, ISP4 CD34-: CD34-negative immature single-positive CD4 cells, EDP CD45high: CD45-high CD34-negative early double-positive cells, LDP: late double-positive cells, SP4: CD4-single-positive cells, rSP4: ready-to-egress CD4-single-positive cells, Treg: T regulatory cells, rTreg: ready-to-egress T regulatory cells, SP8: CD8-single-positive cells, rSP8: ready-to-egress CD8-single-positive cells, T γδ : T γδ cells.

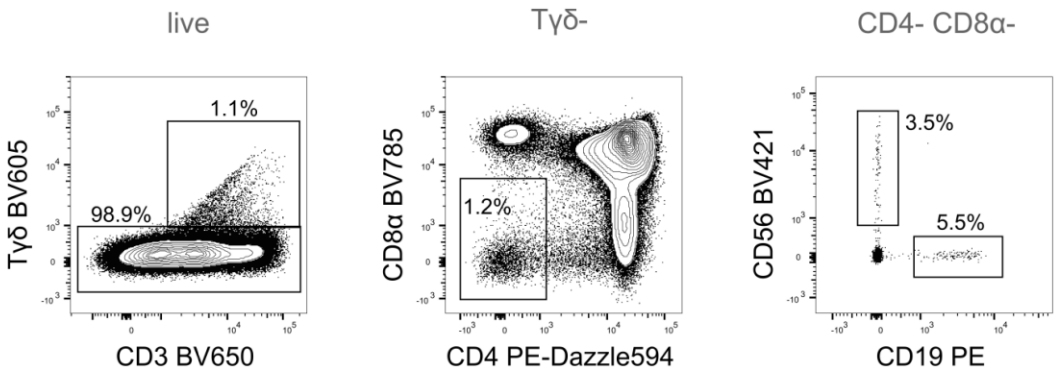

Online Figure 2. Gating strategy for B cells and NK cells in the double-negative compartment of the human thymus. B cells and NK/NKT cells are stained with CD19 and CD56, respectively.

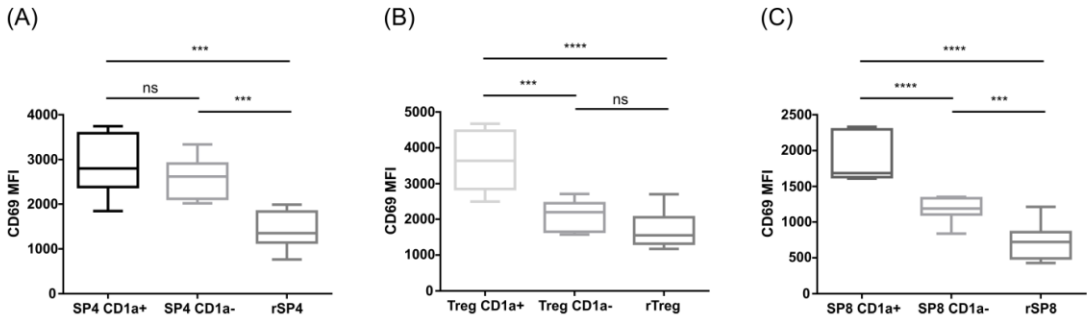

Online Figure 3. Mean fluorescence intensity (MFI) of CD69 in CD4+ cells (A), CD4+ CD25+ T regulatory cells (B) and CD8+ cells (C). Unpaired Student´s *t*-test; ns $p \geq 0.05$, * $p < 0.05$, ** $p < 0.01$, *** $p < 0.001$, **** $p < 0.0001$. N=8

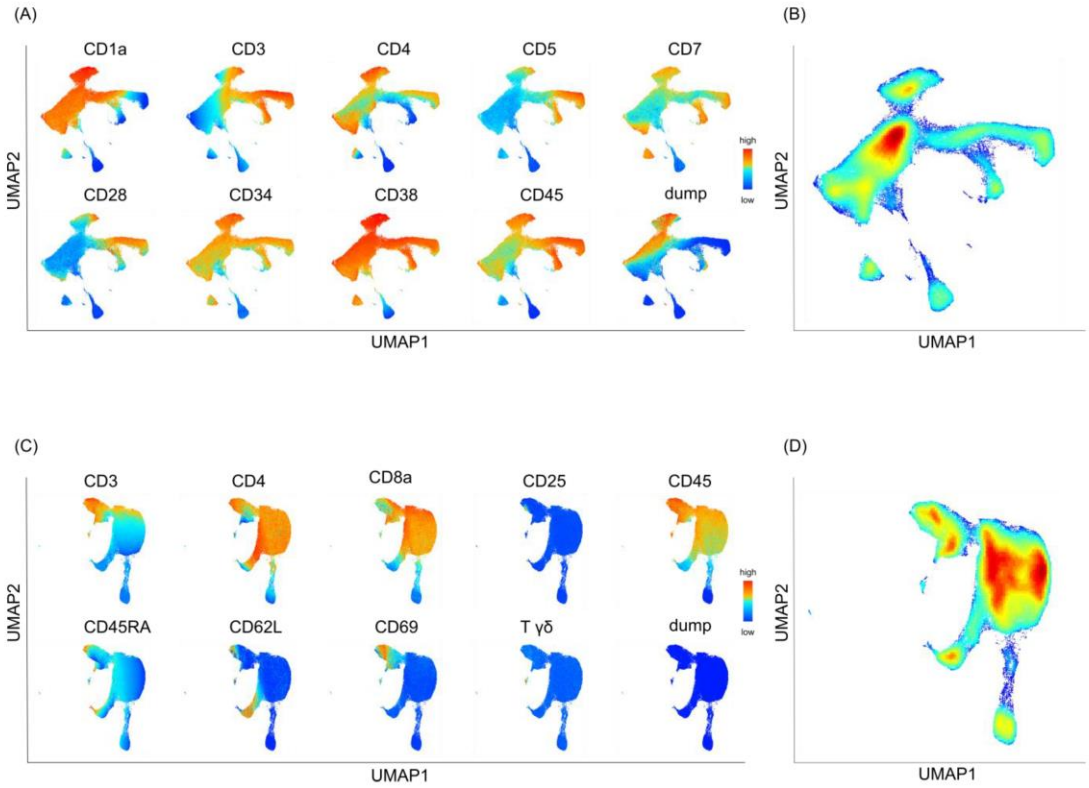

Online Figure 4. UMAP analysis of approx. 110000 cells stained with panel I and panel II, respectively. Depicted is the live cell population. (A) UMAP plots visualizing the expression of each individual cell surface marker of panel I. The dump channel includes CD8β+, CD19+, CD56+ and Tγδ+ cells. (B) UMAP density plot for panel I. (C) UMAP plots visualizing the expression of each individual cell surface marker of panel II. The dump channel includes CD19+ and CD56+ cells. (D) UMAP density plot for panel II.

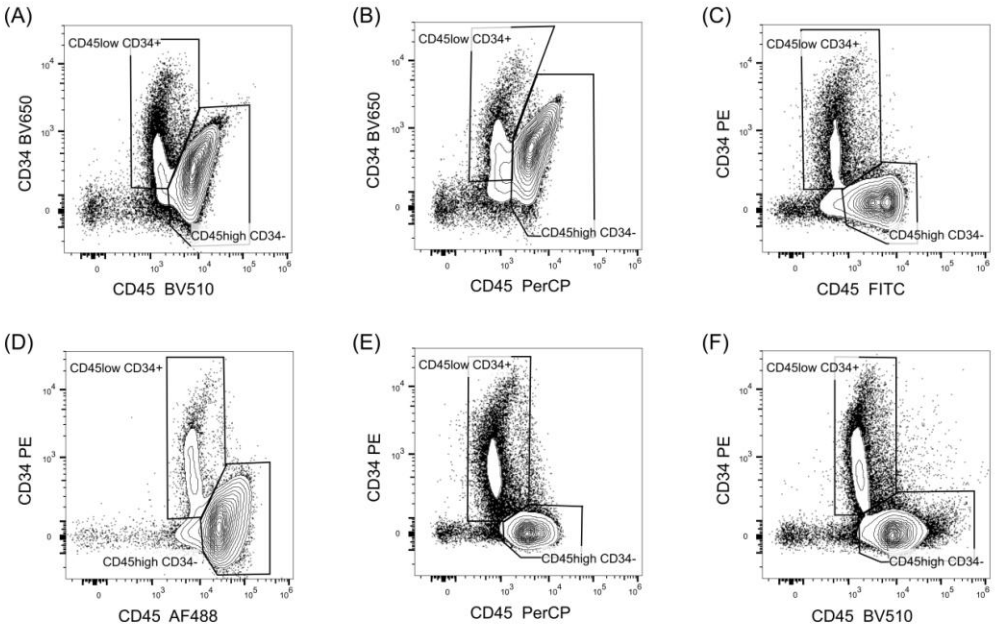

Online Figure 5. Comparison of different reagents for the staining of CD45 and CD34. All stainings were performed together with Annexin V and live/dead staining on human thymocytes. Based on our antibody clone/fluorochrome combination used in panel I (A), we performed optimization processes (B-F) and used the combination with the best separation (F) for our OMIP. (A) CD45-BV510 (clone HI30) and CD34-BV650 (clone 561). (B) CD45-PerCP (clone HI30) and CD34-BV650 (clone 561). (C) CD45-FITC (clone J33) and CD34-PE (clone 563). (D) CD45-AF488 (clone HI30) and CD34-PE (clone 563). (E) CD45-PerCP (clone HI30) and CD34-PE (clone 563). (F) CD45-BV510 (clone HI30) and CD34-PE (clone 563).

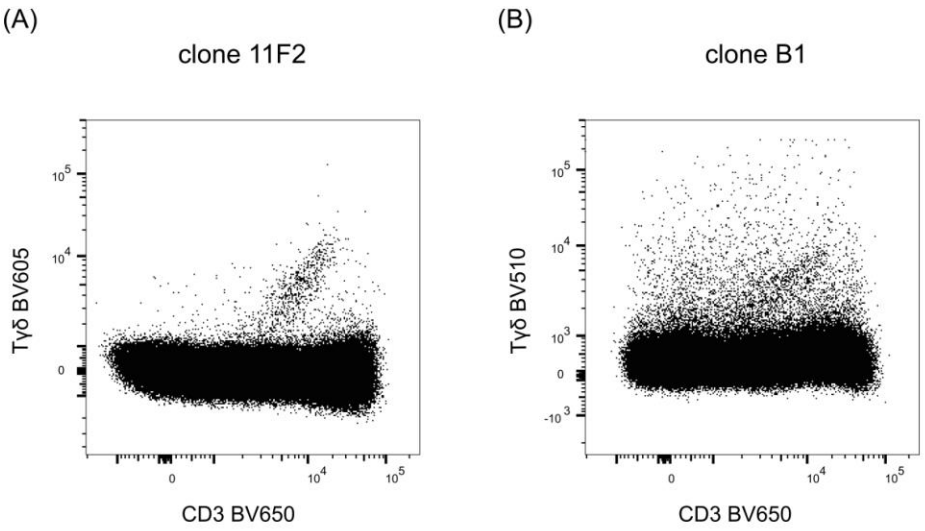

Online Figure 6. Identification of T γδ cells in the human thymus using clones 11F2 (A) and B1 (B). The plots show CD45+ events after exclusion of dead cells and doublets.

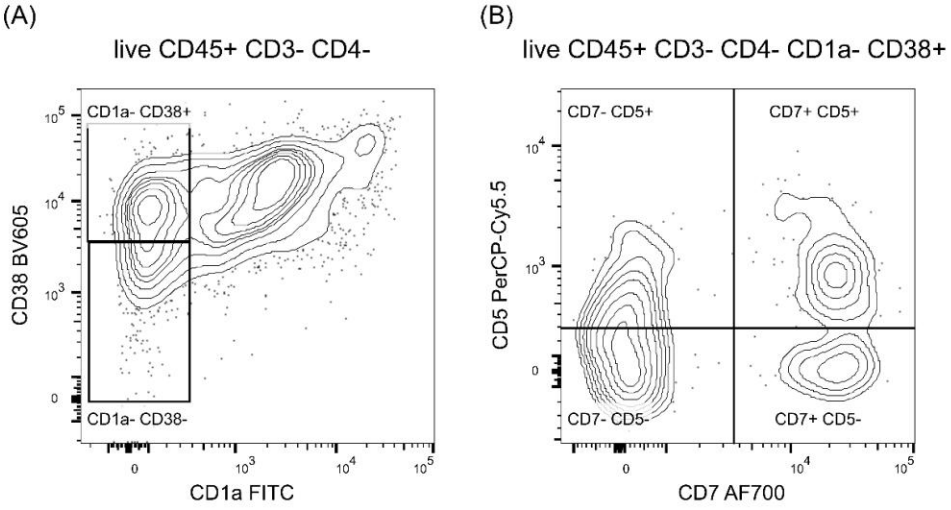

Online Figure 7. (A) Gating of hematopoietic stem cells (CD1a- CD38-) with panel I. Depicted cells are live CD45+ CD3- CD4-. A small population of CD38- cells can be detected within the CD1a- compartment. (B) CD5/CD7 plot to analyze CD38+ cells with panel I before they are T-lineage-committed (CD1a+). Depicted cells are live CD45+ CD3- CD4- CD1a- CD38+.

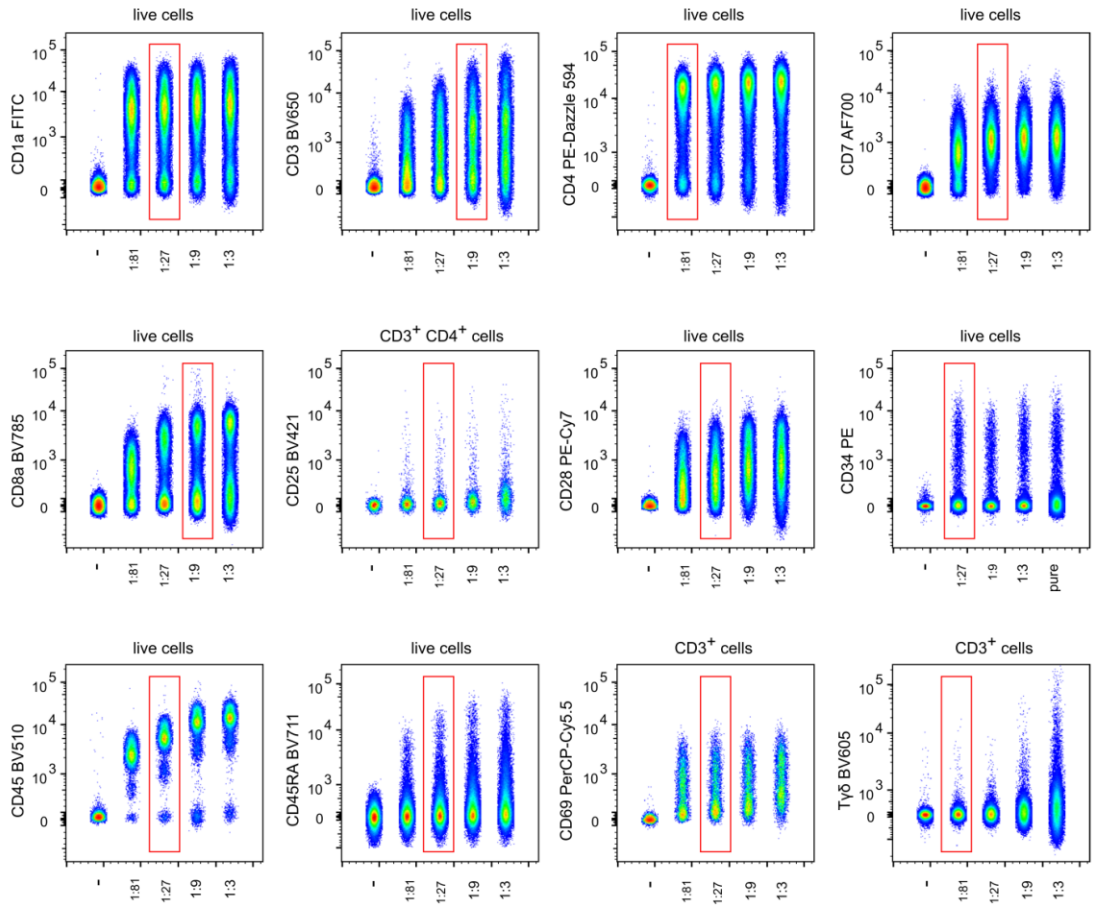

Online Figure 8. Antibody titrations. All antibodies are titrated on 1 million human thymocytes in 1:3 serial dilutions. Titrations were performed in combination with Annexin V and live/dead staining as well as staining of CD3 for the titrations of CD69 and T γδ, and staining of CD3 and CD4 for the titration of CD25. The dilutions used in the panel are framed in red. We calculated the separation index (SI) to select the optimal reagent titers. The SI was calculated using the formula

$$Separation\ Index = \frac{Median\ Positive - Median\ Negative}{(84th\ Percentile\ Negative - Median\ Negative) \div 0.995}.$$

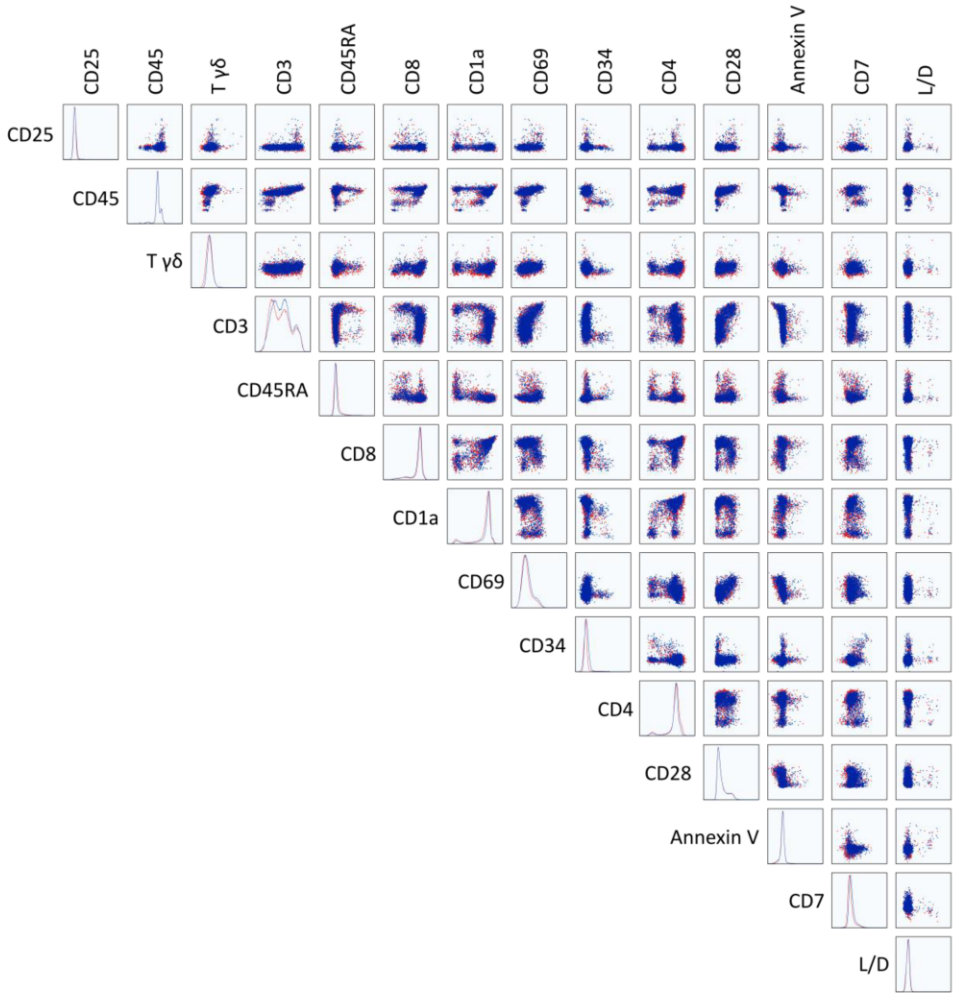

Online Figure 9. NxN plot of single cells stained with the complete thymocyte development panel when compensation matrix was calculated using beads and the same antibodies as in the sample (red overlay) and our alternative approach on fresh thymocytes (blue overlay). For corresponding compensation matrices see Online Table 6.

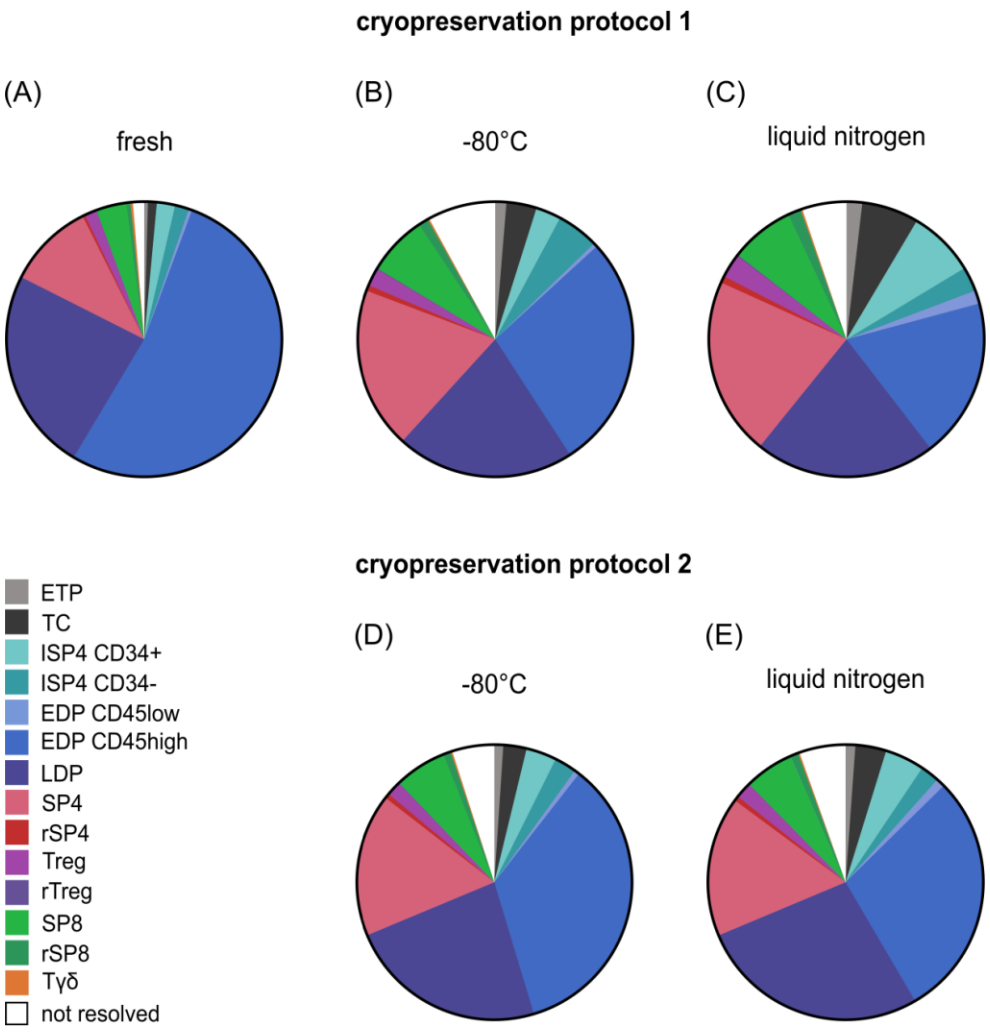

Online Figure 10. Effect of cryopreservation on the distribution of thymocyte subpopulations. The plots show the frequencies of live thymocyte subpopulations (% of total CD45+ cells) in a fresh (A) or for 14 days cryopreserved sample, either kept at -80°C (B, D) or liquid nitrogen (C, E), cryopreserved with protocol 1 (B, C) or protocol 2 (D, E). N=2

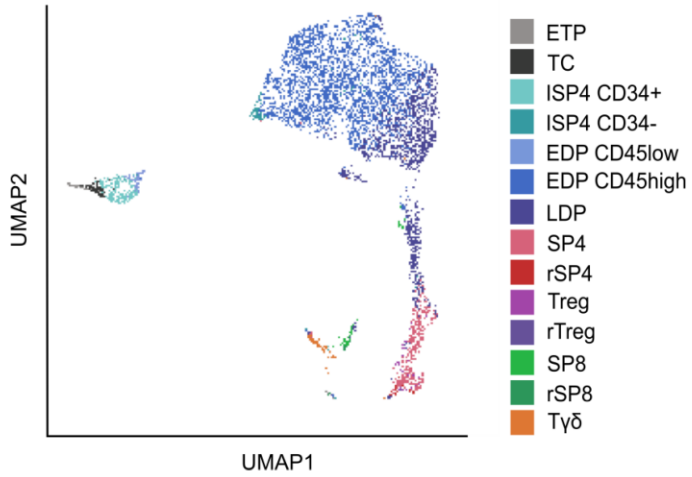

Online Figure 11. Color-coded thymocyte subpopulations after downsampling to 5000 cells. The UMAP overlay plot corresponds to the same representative sample as shown in Figure 1.

Laser	Detector name	LP Filter	BP Filter	Fluorochrome	Antibody	Clone
405nm	V785	750	785/60	BV 785	CD8a	RPA-T8
	V710	680	710/50	BV 711	CD45RA	HI100
	V661	630	661/20	BV 650	CD3	OKT3
	V605	595	605/12	BV 605	Tgd	11F2
	V585	575	585/42			
	V525	475	525/50	BV 510	CD45	HI30
	V450	empty	450/50	BV421	CD25	BC96
488nm	B695	685	695/40	PerCP-Cy5.5	CD69	FN50
	B530	505	530/30	FITC	CD1a	HI149
	SSC	empty	488/10			
561nm	Y780	750	780/60	PE-Cy7	CD28	CD28.2
	Y710	685	710/50			
	Y670	635	670/30			
	Y610	600	610/20	PE-Dazzle594	CD4	RPA-T4
	Y582	575	582/15	PE	CD34	563
640nm	R780	750	780/60	AF750	L/D	
	R730	710	730/45	AF700	CD7	M-T701
	R670	empty	670/14	AF647	AnnexinV	

Online Table 1. Instrument configuration of the cytometer (BD LSR Fortessa).

Fluorochrome	Antibody /reagent	Used dilution (for staining of 1 million cells)	Clone	Company	Catalogue number
BV421	CD25	1:27	BC96	BioLegend (San Diego, CA, USA)	302630
BV510	CD45	1:27	HI30	BioLegend (San Diego, CA, USA)	304036
BV605	Tgd	1:81	11F2	BD Biosciences (San Jose, CA,USA)	745202
BV650	CD3	1:9	OKT3	BioLegend (San Diego, CA, USA)	317324
BV711	CD45RA	1:27	HI100	BioLegend (San Diego, CA, USA)	304138
BV785	CD8a	1:9	RPA-T8	BioLegend (San Diego, CA, USA)	301045
FITC	CD1a	1:27	HI149	BioLegend (San Diego, CA, USA)	300104
PerCP-Cy5.5	CD69	1:27	FN50	BioLegend (San Diego, CA, USA)	310925
PE	CD34	1:27	563	BD Biosciences (San Jose, CA,USA)	550761
PE-Dazzle594	CD4	1:81	RPA-T4	BioLegend (San Diego, CA, USA)	300548
PE-Cy7	CD28	1:27	CD28.2	BioLegend (San Diego, CA, USA)	302926
AF700	CD7	1:27	M-T701	BD Biosciences (San Jose, CA,USA)	561603
AF647	Annexin V	1:5	—	BioLegend (San Diego, CA, USA)	640912
AF750	NHS-Ester (L/D)	1:1000	—	Thermo Fisher Scientific, Waltham (MA), USA	A20011

Online Table 2. Antibodies and reagents used for surface staining.

	BD Celesta				BD LSR Fortessa	
Fluorochrome	**Panel I**	**Clone**	**Panel II**	**Clone**	**OMIP panel**	**Clone**
BV 785	CD3	OKT3	CD45RA	HI100	CD8	RPA-T8
BV 711					CD45RA	HI100
BV 650	CD34	561	CD3	OKT3	CD3	OKT3
BV 605	CD38	HIT2	CD8	RPA-T8	T γδ	11F2
BV 510	CD45	HI30	CD45	HI30	CD45	HI30
BV421	CD4	RPA-T4	CD25	BC96	CD25	BC96
PerCP-Cy5.5	CD5	UCHT2	CD69	FN50	CD69	FN50
FITC	CD1a	HI149	CD62L	DREG-56	CD1a	HI149
PE-Cy7	CD28	CD28.2	T γδ	11F2	CD28	CD28.2
PE-Dazzle594					CD4	RPA-T4
PE	dump: CD19, CD56, T γδ, CD8β	CD19: HIB19, CD56: HCD56, Tγδ: 11F2, CD8β: 2ST8.5H7	dump: CD19, CD56	CD19: HIB19, CD56: HCD56	CD34	563
AF750	live /dead		live / dead		live / dead	
AF700	CD7	M-T701	CD4	OKT4	CD7	M-T701
AF647	Annexin V		Annexin V		Annexin V	

Online Table 3. Panel development. The OMIP is a combination of panel I and panel II.

Fluorochrome	Antibody	Clone	Company	Catalogue Number	Reason for exclusion
BV785	CD3	OKT3	BioLegend	317330	Showed same good separation as CD3-BV650. BV785 was assigned to CD8.
BV421	CD4	RPA-T4	BioLegend	300532	Showed good separation, but CD4-PE-Dazzle594 showed better separation.
PerCP-Cy5.5	CD4	RPA-T4	BioLegend	300530	CD4-BV421 or CD4-PE-Dazzle594 showed better separation.
AF700	CD4	OKT4	BioLegend	317426	Showed low separation. Clone RPA-T4 was given priority due to better separation.
PerCP-Cy5.5	CD5	UCHT2	BioLegend	300619	Was not necessarily needed to gate the defined subpopulations.
BV605	CD8α	RPA-T8	BioLegend	301040	CD8α-BV785 (clone RPA-T8) showed better separation.
PE-Cy7	CD8α	SK1	BioLegend	344712	CD8α-BV785 (clone RPA-T8) showed better separation.
AF700	CD8α	HIT8a	BioLegend	300920	Showed comparable separation to CD8α-BV785.
PE	CD8β	2ST8.5H7	BD Biosciences	641057	Used as dump marker (for mature cells) when analysis was done with two panels. CD8α was given priority.
PE	CD19	HIB19	BioLegend	302208	CD19+ cells only appear in the CD4- CD8- population. Since this population is not further analyzed, there is no need to exclude CD19 with an extra dump channel.
BV650	CD34	561	BioLegend	343623	Switched to the bright fluorochrome PE and clone 563 due to low separation.
PerCP	CD45	HI30	BioLegend	304026	Good separation, comparable to CD45-BV510.
FITC	CD45	J33	Beckman Coulter	AO7782	Good separation, but not ideal in combination with CD34-PE.
AF488	CD45	HI30	BioLegend	304017	Showed low separation.
BV605	CD38	HIT2	BioLegend	303532	Except of an extremely small population, all cells are positive for CD38 in the human thymus. Therefore, CD38 is not needed to gate the defined subpopulations.
BV785	CD45RA	HI100	BioLegend	304140	Showed good separation. CD45RA was assigned to a brighter fluorochrome because of low expression.
PE	CD56	HCD56	BioLegend	318306	CD56+ cells only appear in the CD4- CD8- population. Since this population is not further analyzed, there is no need to exclude CD56 with an extra dump channel.
FITC	CD62L	DREG-56	BioLegend	304804	Was not necessarily needed to gate the defined subpopulations.

PE	Tγδ	11F2	BD Biosciences	333141	Used as dump marker (for mature cells) when analysis was done with two panels.
PE-Cy7	Tγδ	11F2	BD Biosciences	655410	Showed good separation, but PE-Cy7 was assigned to CD28.

Online Table 4. Antibodies tested during optimization but not used in the final OMIP.

Flurochrome	**Antibody**	**Used dilution**	**Clone**	**Company**	**Catalogue number**	**Lot number**
BV605	CD4	1:9	OKT4	BioLegend (San Diego, CA, USA)	317438	#B199792
BV421	CD4	1:9	RPA-T4	BioLegend (San Diego, CA, USA)	300532	#B207664
BV711	CD4	1:9	OKT4	BioLegend (San Diego, CA, USA)	317439	#B181032
PerCP-Cy5.5	CD4	1:27	RPA-T4	BioLegend (San Diego, CA, USA)	300530	#B236220

Online Table 5. Anti-CD4-antibodies used as alternative reagents for the cell-based compensation.

(A)

	CD25	CD45	T γδ	CD3	CD45RA	CD8	CD1a	CD69	CD34	CD4	CD28	Annexin V	CD7	L/D
CD25	100	8.4307	0.8206	0	0.1063	0.0356	1.5787	0.0697	0.3599	0.0469	0	0.4356	0	0.0392
CD45	20.5925	100	59.69	26.0383	8.6306	2.4522	3.6322	0.1211	0	0.0078	0	0	0	0
T γδ	3.0367	0.6397	100	57.5425	16.259	4.5906	1.5396	2.8475	8.2723	23.7362	0.5962	1.084	0	0.1141
CD3	3.0662	0.288	4.3876	100	30.9165	6.9122	0	1.3131	0	1.9008	0.3143	17.9372	6.5374	0.4125
CD45RA	5.6122	1.0194	0.4165	2.6307	100	42.4425	1.7406	16.115	0.6682	0.0581	0.3874	4.6991	48.8593	2.4992
CD8	5.0775	0.2626	0.2501	0	1.5258	100	0.856	0.0906	0	0.0331	0.3315	0.0831	1.2458	1.4211
CD1a	0.0496	0.8813	0.3848	0	0.0869	0.0748	100	0.6563	0.2632	0.0548	0	0.3022	0	0
CD69	0.2099	0.1166	0.3265	8.8146	25.3711	7.8592	2.5751	100	0.8447	0.1648	1.7718	28.6312	23.3317	1.4969
CD34	1.1433	1.6333	6.8326	3.4299	0.7622	0.1641	9.49	11.0287	100	50.5051	0.5291	1.9885	0	0.3214
CD4	0	0	7.9338	3.3414	1.1443	0.252	0.6614	26.9986	13.2709	100	1.1121	0.0619	0.0113	0
CD28	0.3787	0.284	0.426	0	0.142	19.4576	2.3761	0.5589	3.4714	1.8821	100	0.4541	2.2006	4.8203
Annexin V	0	0	0.0266	0	0.1598	0	0.6077	0.3752	0	0.1177	0	100	30.7753	1.3363
CD7	1.0968	1.1516	0.6946	0.6032	4.3506	1.9382	3.7369	1.8507	1.5181	0.2746	0.9206	6.0426	100	4.2352
L/D	0	0	0	0	0.6924	72.3209	1.5836	0.3589	0.0852	0.6117	21.4944	9.299	61.4718	100

(B)

	CD25	CD45	T γδ	CD3	CD45RA	CD8	CD1a	CD69	CD34	CD4	CD28	Annexin V	CD7	L/D
CD25	100	12.2227	0.6926	0.2309	0.0389	0.0251	0.0334	0	0	0.004	0.004	0.0059	0	0.0084
CD45	13.1528	100	41.274	27.016	5.0279	2.5929	0.4046	0.0333	0	0.0054	0	0.0224	0	0.0134
T γδ	3.158	0.4657	100	84.7482	13.8789	6.7745	0.0044	1.8373	4.1187	18.2794	0.8786	0.2613	0.0884	0.0179
CD3	2.4321	0.5001	3.2845	100	18.0475	7.2281	0.0311	0.6016	0.01	1.0342	0.251	14.3732	5.7374	0.3941
CD45RA	6.9137	1.2228	0.239	4.7623	100	71.6696	0.0923	12.8876	0	0	0.7716	5.834	76.1009	5.3388
CD8	4.0248	0.6313	0.17	0.3491	0.9409	100	0.0111	0.0194	0.008	0.0107	0.4747	0.1747	1.184	1.9373
CD1a	0.0392	5.2322	0.8381	0.3799	0.0548	0.0235	100	1.4225	0	0	0	0.0144	0	0
CD69	0.0562	0.1236	0.0449	22.3418	31.7965	17.8083	0.0205	100	0	0.0099	4.1989	45.4225	37.5275	3.0508
CD34	0.0735	0.2834	12.279	5.5937	0.8816	0.2729	1.8294	14.0219	100	74.5387	1.0385	0.1007	0	0.031
CD4	0.0186	0.0345	11.5092	8.3566	1.5232	0.6024	0.1768	24.4776	9.6338	100	2.2672	0.2741	0.0875	0.0059
CD28	0.037	0.0741	0.1575	0.1111	0.1297	23.2709	0.2071	0.4649	1.1211	0.9697	100	0.082	2.2405	5.3682
Annexin V	0	0	0	0.0968	0	0	0.2651	0.1105	0	0	0.5133	100	33.6492	2.751
CD7	0.0476	0.0951	0.0555	0.1348	3.0051	2.0774	0.0289	0.7164	0	0.021	1.0928	2.7614	100	5.359
L/D	0	0	0	0	0.2552	64.5214	0.2117	0.0847	0	0.1435	20.5658	0	47.708	100

Online Table 6. Compensation matrices generated with FlowJo using single-fluorochrome stained fresh thymocytes (A) or beads (B). For the cell-based compensation (A) the same antibodies that are used in the panel were used for CD1a, CD3, CD4, CD7, CD8a, CD28, CD34, CD45, live/dead and Annexin V and alternative CD4-conjugates listed in Online Table 5 were used for CD25, CD45RA, CD69 and T γδ. For the bead-based compensation (B) we used the original antibodies listed in Online Table 2. The compensation of live/dead and Annexin V was always (A, B) performed on cells.

Population	Mean	SD	Max	Min
	% of CD45+			
ETP	0.61	0.33	1.3	0.36
TC	1.17	0.61	2.38	0.53
ISP4 CD34+	3.39	1.36	4.82	1.34
ISP4 CD34-	1.4	0.63	2.7	0.61
EDP CD45low	1.17	0.51	1.82	0.5
EDP CD45high	53	5.45	61.4	47.2
LDP	25.8	3.16	29.8	22.2
SP4	7.32	1.61	10.6	5.42
rSP4	0.66	0.34	1.39	0.39
Treg	0.76	0.29	1.33	0.31
rTreg	0.12	0.045	0.18	0.04
SP8	2.57	1.1	4.24	1.16
rSP8	0.32	0.26	0.94	0.11
Tgd	0.58	0.35	1.18	0.18
not resolved	1.13	0.46	1.83	0.46

Online Table 7. Average frequencies of thymocyte subsets, calculated from 8 human pediatric thymi aged 6-12 months.

Reagents	**Company**	**Catalogue Number**
NaCl	Fisher Scientific, Hampton (NH),USA	BP358-1
$CaCl_2$	Fisher Scientific, Hampton (NH),USA	AC349610250
Hepes	PAA Laboratories, Pasching, Austria	S11-001
Dulbecco's Phosphate-Buffered Salines (DPBS) (10x)	GibcoTM, Paisley, UK	14190-094
Bovine Serum Albumin (BSA)	PAA Laboratories, Pasching, Austria	K41-001
NaN_3 99%	Roth, Karlsruhe, Germany	K305.1
X-Vivo 15 medium	Lonza, Basel, Switzerland	BE02-060F
RPMI 1640	Thermo Fisher Scientific, Waltham (MA), USA	12633012
Fetal bovine serum (FBS)	Biochrom, Berlin, Germany	S0615
DNase I	Qiagen, Hilden, Germany	1010395
Dimethyl sulfoxide (DMSO)	AppliChem, Darmstadt, Germany	A3672,0100
Trypan blue solution, 0.4%	Sigma-Aldrich, St.Louis (MO), USA	T8154

Online Table 8. Reagent information.

Materials	Company	Catalogue Number
Cell strainer, nylon, 70µm	Falcon, Corning Incorporated, Corning (NY), USA	352350
Cellstar tubes 15 ml	greiner bio-one, Kremsmünster, Austria	188271
Cellstar tubes 50 ml	greiner bio-one, Kremsmünster, Austria	227261
Falcon, 5 ml, round-bottom tube	Falcon, Corning Science Mexico, Reynosa, Mexico	352052
Neubauer improved	Marienfeld superior, Lauda-Königshofen, Germany	640010
CryoTubeTM Vials	Thermo Fisher Scientific, Waltham (MA), USA	368632
Mr. Frosty™ Freezing container	Fisher Scientific, Hampton (NH), USA	10110051

Online Table 9. Materials used for this OMIP.

	Abbreviation	Explanation
Thymocyte populations	ETP	early thymic progenitors
	TC	T-lineage-committed cells
	ISP4	immature single-positive CD4-positive cells
	EDP	early double-positive cells
	LDP	late double-positive cells
	SP4	CD4-single-positive cells
	rSP4	ready-to-egress CD4-single-positive cells
	Treg	T regulatory cells
	rTreg	ready-to-egress T regulatory cells
	SP8	CD8-single-positive cells
	rSP8	ready-to-egress CD8-single-positive cells
	Tγδ	T γδ cells
Fluorochromes	BV	Brilliant Violet
	PerCP	Peridinin Chlorophyll
	PerCP-Cy5.5	Peridinin Chlorophyll - Cyanine5.5
	FITC	Fluorescein isothiocyanate
	PE-Cy7	Phycoerythrin-Cyanine7
	PE	Phycoerythrin
	AF	Alexa Fluor
Other reagents	HEPES	4-(2-hydroxyethyl)-1-piperazineethanesulfonic acid
	PBS	phosphate-buffered saline
	BSA	bovine serum albumin
	RPMI	Roswell Park Memorial Institute
	FBS	fetal bovine serum
	DMSO	dimethyl sulfoxide
Others	RT	room temperature
	FSC-A	Forward Scatter-Area
	SSC-A	Side Scatter-Area
	FSC-H	Forward Scatter-Height
	SSC-H	Side Scatter-Height
	PMT	photomultiplier tube
	LP	long pass
	BP	band pass
	UMAP	Uniform Manifold Approximation and Projection
	t-SNE	t-distributed stochastic neighbor embedding

Online Table 10. Abbreviations

2 DESCRIPTION OF THE PUBLICATION AND FURTHER RESULTS

2.1 INTRODUCTION

2.1.1 Human T cell development in the thymus

Before Jaques Miller identified the thymus as a key player in the development of the adaptive immune response in 1961 (2) and its role in providing a pool of immunocompetent cells (3), the thymus was thought to be a vestigial organ and a "graveyard for dying lymphocytes" (4). After 60 years of research, we have made important progress in the elucidation of the stages of thymocyte maturation and the regulation of T cell development in the murine system. However, a consistent translation to the human system is still missing.

The thymus provides the microenvironment for developing T cells. Haematopoietic precursors migrate from the bone marrow and enter the thymus at the cortico-medullary junction (5). These precursors express CD34, a marker of haematopoietic stem and progenitor cells (6), and low levels of CD45 (7). Upon interaction with Notch ligands on thymic epithelial cells (TECs), Notch is activated and leads to the upregulation of T cell specific genes (8). The loss of CD44 and the expression of CD1a mark T lineage commitment (7). Within the CD34+ CD1a+ compartment, thymocyte populations can be defined by expression of CD4 and CD8. Early T lineage-committed cells are CD4- CD8-, human immature single-positive cells express CD4 (ISP4) and a small fraction of cells is positive for CD4 and CD8 while still expressing low levels of CD45 (early double-positive (EDP) CD45low) (1). During these early developmental steps, the rearrangement of the T cell receptor (TCR) loci is initiated (9). The vast majority of thymocytes will finally express a functionally rearranged αβ receptor (10), but a small proportion of about 0.6 % will develop into T cells harbouring a γδ TCR (1). The final downregulation of CD34 coincides with the full expression of CD45. The earliest population within the CD45high CD34- compartment is a population of ISP4 cells that can be subdivided in cells pre and post β-selection checkpoint with the help of CD28 (11). The CD4+ CD8+ double-positive (DP) subset represents the largest cell population in the thymus with about 80 % of the thymocytes. Early DP (EDP) thymocytes express low levels of CD3, while in late DP (LDP) cells CD3 expression is high (1). To generate a self-referent and – at the same time – non-autoreactive TCR repertoire, thymocytes are thoroughly selected according to the affinity of their TCR for self-antigens presented by MHC molecules: If they cannot interact with self-peptide-MHC complexes on TECs, they die by neglect. If the TCR has an intermediate affinity for self-peptide-MHC complexes, the cell is positively selected; if the affinity is intermediate-high, regulatory T cell differentiation is induced; and if the affinity is too high, the cell is negatively selected to prevent autoreactivity (12). Depending on the specificity and signal strength of the TCR to MHC class I or MHC class II molecules, thymocytes further differentiate into single-positive (SP) cytotoxic CD8+ T cells or helper CD4+ T cells, respectively (13). When thymocytes are ready to egress the thymus and migrate to the periphery as recent thymic emigrants, they lose their tissue retention marker CD69 and upregulate CD45RA (14).

Already at 10 weeks of gestation, the foetal thymic rudiment is colonized by haematopoietic precursors (15). The thymus is most active during the prenatal period and within the first year of life and begins to involute afterwards. Involution starts slowly and accelerates after adolescence (16–18). Although thymic involution results in decreased T cell generation, naïve T cells and T cell receptor

excision circles (TREC) are still found in the blood of elderly individuals, reflecting maintained output (19).

2.1.2 Endogenous and exogenous glucocorticoids during early life and their effects on the thymus

Glucocorticoids (GCs) are endogenously produced, mainly in the adrenal glands, regulated by the hypothalamic-pituitary-adrenal axis. They regulate ~20 % of the genome (20) and are involved in a variety of physiological processes like development, metabolism or inflammation. GCs execute genomic effects upon nuclear translocation of the glucocorticoid receptor (GR) as well as non-genomic effects following ligand-induced dissociation of the GR multiprotein complex. As immunomodulators, GCs downregulate pro-inflammatory cytokines, upregulate anti-inflammatory cytokines, alter the polarization of T cells and therefore, are widely used for treatment of inflammatory and autoimmune disorders (immunoregulatory effects of GCs reviewed in (21)).

2.1.2.1 T cell development and glucocorticoids

Developing thymocytes are extremely sensitive to GC-induced cell death (22). During the prenatal period, GC levels can be elevated due to high maternal stress levels (endogenous GCs), treatment of acute inflammatory conditions, or antenatal GC administration to induce foetal lung maturation (exogenous GCs) (23). In addition, GCs are locally synthesized in the thymus (24). Highly elevated systemic GC levels after exogenous administration or enhanced adrenal production result in apoptosis of thymocytes and massive involution of thymic tissue. Interestingly, DP thymocytes are most sensitive to GCs although they express the lowest GR levels (25). Here, the expression of the pro-apoptotic proteins Bim (Bcl-2-interacting mediator of cell death), which is required for negative selection (26), and Puma (p53-upregulated modulator of apoptosis) contributes to apoptosis of thymocytes (27). Endogenous GCs do not only cause apoptosis of thymocytes, they also influence selection processes. Local GC production by TECs promotes positive selection and allows thymocytes with a TCR with high affinity for self-antigens to survive (24,28) by inhibiting Nur77 and Helios (transcription factors involved in negative selection) (29). Moreover, TEC-derived GCs specifically target CD4+ CD8+ TCRhigh cells and this DP subset is exposed to higher GC levels than other thymocytes (30) (GCs and T cell development reviewed in (28)).

2.1.2.2 Prenatal glucocorticoid treatment

A special case of exogenous GC exposure early in life is the prenatal administration of GCs (betamethasone or dexamethasone). Pregnant women at risk of early delivery between the 24th and 34th week of gestation receive GCs in order to accelerate the maturation of the foetal lung. This treatment reduces respiratory distress syndrome (RDS) and the need for mechanical ventilation, and results in reduced neonatal mortality (31,32). Besides these undisputed beneficial effects, little is known about possible side effects, especially on the sensitive thymocytes. In contrast to endogenous GCs, both betamethasone and dexamethasone cross the placenta readily and are poor substrates for inactivation by placental 11ß-HSD2 enzyme. In addition, they are poor binders to the corticosteroid-binding globulin and have a higher affinity to the intracellular GR than other GCs (23). Imaging of the foetal thymus upon prenatal GC treatment revealed impaired foetal thymus growth (33,34). Epidemiological studies have shown that prenatal betamethasone administration is associated with a transient immunosuppression in very low birth weight infants (35) and that multiple courses

(>2 doses) of betamethasone are associated with early-onset neonatal sepsis and other infectious morbidities (36). Additionally, there is evidence that prenatal GCs might increase the risk of developing asthma (37) and type 1 and 2 diabetes in children (38). In mice, perinatal GC exposure causes long-term effects on CD8 T cell function, hampering the control of bacterial infections and tumour growth (39). Our group has previously demonstrated in a mouse model that prenatal GC treatment causes massive reduction in thymic volume of the offspring, induces apoptosis of thymocytes, mainly in the DP compartment, and leads to changes in the TCR repertoire (40,41).

2.1.2.3 The thymus in children with congenital heart disease

The source of thymic tissue for studies on human T cell development is usually discarded tissue from corrective cardiac surgery performed on children with congenital heart disease (CHD). Because of the lack of control tissue, it is not known if CHD *per se* has a direct effect on T cell development. Hypoxia induces an increase in corticosterone levels in animal models (42,43), and GCs influence the adaptation to hypoxic environments and upregulate HIF-1-dependent (hypoxia-inducible factor 1) gene expression (44). The thymus volume (adjusted for foetal weight and gestational age) of foetuses with CHD is significantly decreased compared to healthy controls (45), but the levels of cortisol in the serum of infants with cyanotic and acyanotic CHD are comparable (46). Interestingly, there is a correlation between low oxygen saturation (SpO_2 < 95 %) and low TREC numbers (47), indicating reduced thymic output in conditions of cyanosis.

2.2 MATERIALS AND METHODS

2.2.1 Materials

2.2.1.1 Thymic tissue and plasma

Sample	Source	Ethic approval	Info
Thymus & Plasma	Surgery for Congenital Heart Disease, University Heart & Vascular Center Hamburg, University Medical Center Hamburg-Eppendorf, Hamburg, Germany	PV5482	Plasma was taken in the morning at the beginning of general anaesthesia
Plasma (control group)	Plasma samples were kindly provided by Dr. Mats Ingmar Fortmann from UKSH (Campus Lübeck) and obtained under local ethic approval.		

2.2.1.2 Cell lines

OP9 stromal cells expressing no Notch ligand, delta-like ligand 4 (OP9-DL4) or delta-like ligand 1 (OP9-DL1) where kindly provided by Prof. Tom Taghon, Ghent University.

2.2.1.3 Media and Buffer

Buffer	Composition
Annexin V buffer (10x)	H_2O with 1.4 M NaCl, 25 mM $CaCl_2$, 0.1 M HEPES
FACS buffer	1x PBS with 0.1 % BSA, 0.02 % NaN_3
MACS buffer	1x PBS with 0.5 % BSA, 2 mM EDTA
OP9 medium	H_2O with 10 g/l MEM Alpha Medium, 20 % FCS, 100 U/ml penicillin, 100 µg/ml streptomycin, 2 mM L-Glutamine, 2.2 g/l $NaHCO_3$

2.2.1.4 Reagents, solutions and kits

Reagents and solutions	Company
Annexin V Binding Buffer (10x)	EXBIO Praha, a.s., Czech Republik
Bovine Serum Albumin	PAA Laboratories, Pasching, Austria
Betamethasone	Sigma-Aldrich, St. Louis (MO), USA
Dulbecco's Phophate-Buffered Saline (DPBS) (10x)	GibcoTM, Paisley, UK
Ethanol ≥ 99,8 %	Roth, Karlsruhe, Germany
Fetal Bovine Serum	Biochrom, Berlin, Germany
Human recombinant IL-7	R&D Systems, Inc., Minneapolis (MN), USA
Human FLT3-Ligand	Miltenyi Biotec, Bergisch Gladbach, Germany
L-Glutamine (200 mM)	GibcoTM, Paisley, UK
MEM Alpha Medium	GibcoTM, Paisley, UK
NaN_3 99 %	Roth, Karlsruhe, Germany
$NaHCO_3$	Biochrom GmbH, Berlin, Germany
RU-486	Sigma-Aldrich, St. Louis (MO), USA
SCF (recombinant human)	PeproTech, Hamburg, Germany
Streptomycin (10.000 µg/ml) / Penicillin (10.000 U/ml)	GibcoTM, Paisley, UK
Trypan blue solution, 0.4 %	Sigma-Aldrich, St. Louis (MO), USA
Trypsin-EDTA, 0.5 % (10x)	Thermo Fisher Scientific, Waltham (MA), USA
Tuerck's solution	Sigma-Aldrich, St. Louis (MO), USA
X-Vivo 15 medium	Lonza, Basel, Switzerland

Kits	Company	Catalogue Number
CD34 MicroBead Kit UltraPure	Miltenyi Biotec, Bergisch Gladbach, Germany	130-100-453
Cortisol Competitive ELISA Kit	Thermo Fisher Scientific, Waltham (MA), USA	EIAHCOR

2.2.1.5 Antibodies

For antibodies of the T cell development panel, see the published supplementary material page 30 of *Bremer et al.*(1).

Antibody	Fluorochrome	Clone	Company	Catalogue number	Panel
CD34	PE	563	BD Biosciences	7129824	Purity test after MACS
Live/Dead	AF750		Thermo Fisher	A20011	

2.2.1.6 Software

Software	Company
BD FACSDiva	Becton Dickinson, Franklin Lakes (NJ), USA
BioRender	BioRender.com
FlowJo 10.7.1 software	FlowJo, LLC, Ashland, USA
GraphPad Prism 9	GraphPad Software, Inc., La Jolla, USA
Inkscape vector graphics editor	Inkscape.org
Mendeley Desktop 1.19.8	RELX Group, London, United Kingdom
Microsoft Office 2010	Microsoft, Redmond (WA), USA

2.2.2 Methods

2.2.2.1 Tissue preparation

For a detailed protocol of the isolation of thymocytes, see page 16 of the published supplementary material.

2.2.2.2 Cryopreservation and thawing

The protocols for cryopreservation and thawing are provided in the published supplementary material, pages 17-18.

2.2.2.3 Surface staining for flow cytometry

The protocol for the staining of specific surface markers with fluorochrome-conjugated antibodies is provided in the published supplementary material, pages 16-17.

2.2.2.4 Cortisol competitive ELISA

The cortisol competitive ELISA was performed according to the manufacturer's instructions.

2.2.2.5 MACS-isolation of CD34+ thymocytes

CD34+ thymocytes were isolated with the 'CD34 MicroBead Kit UltraPure' according to the manufacturer's instructions.

2.2.2.6 Betamethasone overnight incubation

One million thymocytes per well were cultured in a 48-well-plate for 16 hours at 37 °C in a volume of 400 µl x-vivo 15 medium with increasing concentrations of betamethasone (0 nM, 1 nM, 10 nM, 100 nM, 1 µM). For betamethasone overnight incubation with RU-486, RU-486 was added to the respective wells with a final concentration of 1 µg/ml. The next day, cells were harvested, counted, washed with 1 ml Annexin V buffer and stained with the panel published in OMIP 073. Cells were analysed on a BD LSRFortessa flow cytometer.

2.2.2.7 OP9 coculture system

Thawing of OP9 cells

OP9, OP9-DL1 and OP9-DL4 cells were quickly thawed in a water bath (37 °C) and transferred to a tube with 10 ml OP9 medium. They were centrifuged (1500 rpm, 5 min, RT), resuspended in OP9 medium and transferred into a small flask that was placed in the incubator (37 °C, 5 % CO_2).

Maintaining OP9 cell culture

The cells were passaged at about 70 % confluency to avoid formation of adipocytes. To passage the cells, OP9 medium was removed and the flasks were washed with 10 ml of DPBS. The cells were treated with 1.5 ml of 0.25 % trypsin solution and incubated for 3 min at 37°C. Afterwards, the cells were disaggregated with 4 ml OP9 medium and transferred into a tube for centrifugation (1500 rpm, 5 min, RT). The cells were resuspended in 1 ml OP9 medium, counted and 0.5×10^6 cells were transferred in a new flask containing 10 ml OP9 medium.

OP9 coculture with thymocytes

OP9, OP9-DL1 and OP9-DL4 cells were seeded in a 24 well-plate (100,000 cells/well, total volumes of 500 µl OP9 medium per well) and incubated overnight (37 °C) so that they had generated a confluent layer the next day. One well was prepared for each analysis time point and condition (bet+ and bet-). Thymocyte single-cell suspension was used for MACS-isolation of CD34+ cells and purity was tested by FACS (stained with anti-CD34 PE and live/dead AF750). Isolated cells were either frozen (see OMIP 073 "Cryopreservation and thawing") or directly incubated. MACS-isolated CD34+ fresh or thawed cells were incubated with 0 nM and 10 nM betamethasone, respectively, in a 48-well-plate for 16 hours at 37°C in a volume of 400 µl OP9 medium. The next day, cells were washed, counted and 5000-10000 CD34+ cells of both conditions (bet+ and bet-) were analysed by FACS with the T cell development panel. The rest of the purified CD34+ cells was resuspended in the appropriate volume of OP9 medium (4000-30000 cells/well, 500 µl medium/well) which was supplemented with the required cytokines (10 ng/ml SCF, 5 ng/ml FLT3-L, 10 ng/ml IL-7). The medium from the confluent OP9 cells was removed and 4000-30000 CD34+ cells in 500 µl

supplemented OP9 medium were seeded onto the OP9, OP9-DL1 or OP9-DL4 cell layer. Coculture plates were placed in an incubator (37 °C). Thymocytes were analysed every 5 days. Therefore, cells from each condition (bet+ and bet-) were pooled, counted, and the cell count of one well was stained with the T cell development panel and analysed by FACS on a BD LSRFortessa flow cytometer. Remaining cells were split and seeded on OP9 monolayers that have been freshly prepared the day before (one well for each condition and remaining analysis time point).

2.3 RESULTS

2.3.1 Establishment of an "Optimized Multicolor Immunofluorescence Panel" (OMIP) for the analysis of human thymocyte development

Flow cytometry is a powerful tool to analyse the phenotype of cells based on the expression of specific markers. The development of new dyes and the availability of multi-laser flow cytometers permit the analysis of an ever increasing number of parameters, and panel design has become a challenging task. Staining panels for detecting specific immune cell subpopulations, known as OMIPs, are continuously developed to share practical knowledge of novel, intensively optimized fluorochrome-conjugated antibody combinations to address specific research questions (48). In this thesis, I want to present OMIP 073, entitled "Analysis of human thymocyte development with a 14-color flow cytometry panel" that was developed in order to define thymocyte subpopulations and assess their frequencies in the human system (1). This FACS panel is used in our lab to assess thymocyte subpopulations in healthy and diseased cases *ex vivo* (Figure 1), in short term assays, and in *in vitro* models of T cell development.

Here, I will present the use of this panel to investigate two conditions that are likely to impair T cell development in early life: 1) exposure to exogenous GCs modelling prenatal steroid treatment, and 2) exposure to endogenous GCs due to congenital heart disease.

2.3.2 *In vitro* effects of betamethasone on T cell development

2.3.2.1 Betamethasone treatment induces thymocyte apoptosis and alters subset composition

To investigate the effect of betamethasone on human thymocytes *in vitro*, we incubated thymocytes obtained from fresh thymic tissue with increasing concentrations of betamethasone. FACS analysis of the thymocyte subpopulations was performed with the panel described in OMIP 073, including Annexin V staining for detection of apoptotic cells. Treatment with 10 to 1000 nM betamethasone resulted in increasing rates of apoptotic death of thymocytes that could be prevented by adding the GR-antagonist RU-486 (Figure 2 A-B). Immature CD45low CD34+ thymocytes are highly susceptible to GC-induced cell death. Among the most immature subsets, ISP4 CD34+ thymocytes showed a significant decrease from an average of 26.49 % (0 nM) to 17.60 % of CD45low CD34+ cells already with 10 nM betamethasone. Within the CD45high CD34- compartment, predominantly DP cells underwent apoptosis (81.76 % (0 nM) to 63.63 % (1000 nM) of CD45high CD34- cells). That led to a relative increase of the frequencies of T regulatory, CD4 SP and CD8 SP cells (Figure 2 C-D). We used the dimensionality reduction algorithm t-distributed stochastic neighbour embedding (t-SNE) to visualize the co-expression of markers on each cell, and identified markers associated with a survival

advantage (CD28 and CD45RA) or with an increased risk for GC-induced apoptosis (CD7 and CD34) (Figure 2 E).

2.3.2.2 Betamethasone treatment delays thymocyte development

We further analysed the effect of betamethasone on the dynamics of T cell development using the OP9 coculture system (Figure 3 A-C). OP9 cells are stromal cells that support haematolymphopoiesis and induce T cell differentiation when expressing an appropriate Notch ligand (49). We used delta-like-4-expressing OP9 cells (OP9-DL4), because in our pilot experiments thymocyte proliferation was higher with OP9-DL4 than with OP9-DL1. Thymus-derived CD34+ cells were given a 16h pulse of betamethasone to mimic prenatal steroid administration and then cocultured with OP9 cells. Thymocytes proliferated until day 10, afterwards cell numbers started to decrease. Control cultures showed proliferation advantages with significantly more developing thymocytes after 10 days of culture (Figure 3 B). After 5 days of culture, most of the thymocytes were double-negative (DN) for CD4 and CD8 expression (bet+: 68.5 %, bet-: 58.3 %), and a fraction of thymocytes already developed into ISP4 cells (bet+: 7.0 %, bet-: 19.4 %). We observed development of ISP8 cells in both groups that do not (or to a far lesser extent) exist in human *in vivo* T cell development. From day 5 to 20, the frequencies of DP cells steadily increased in both groups with a delayed DP cell development in the betamethasone-exposed group (day 20: bet+: 33.1 %, bet-: 44.3 %). Concomitantly, we observed a decrease of DN cells and an increase of CD8 SP cells in both groups, with higher frequencies in the betamethasone-exposed group. The frequency of CD4 SP cells declined in the betamethasone-exposed group after day 15 and in the control group from day 5 onwards. This can be most likely explained by the development of ISP4 cells into DP cells and a delay in the betamethasone-exposed group (Figure 3 C). In summary, we were able to generate DP as well as CD4 and CD8 SP thymocytes in the OP9 coculture system and showed that betamethasone exposure affects thymocytes by delaying their development.

2.3.3 The thymus in the context of age and disease

We assessed the composition of thymocytes in 44 children of different ages affected with different cardiac conditions (Table 1). Cases with very severe heart defects, such as transposition of the great arteries (TGA), hypoplastic left heart syndrome or aortic stenosis, are generally operated at an earlier age than less severe heart defects like ventricular or atrial septal defects (VSD/ASD) or Tetralogy of Fallot (ToF). We found a lower frequency of DP thymocytes in the thymi of the youngest infants (< 1 month of age) concomitant to higher frequencies of the SP populations (CD8+ cells, CD4+ cells and T regulatory cells). Interestingly, the youngest children showed the most heterogeneous thymocyte compositions (Figure 4). The comparison of thymocyte subsets between the different heart condition groups revealed a reduction of the DP compartment and a relative increase of CD4 SP thymocytes in the most severe disease groups, namely TGA and a group summarised as “left hypoplasia”, which could indicate physiological stress (Figure 5). Levels of NT-proBNP, a biomarker for heart failure (50), correlated negatively with the frequencies of DP cells and more immature EDP CD45low cells and positively with the frequencies of CD4+ and T regulatory cells (Figure 6). Comparable results were seen for the correlation of Troponin T, a marker for myocardial damage (51), and thymocyte subsets (data not shown).

The composition of thymocytes in severe CHD is reminiscent of the picture that we observed in thymocytes following betamethasone treatment. Different stress stimuli like infection or injury induce

adrenal GC production and subsequent thymic involution and DP depletion (28). For this reason, we measured the cortisol levels in the plasma of children undergoing corrective cardiac surgery and in healthy children of similar ages. Regression analysis showed no significant correlation between cortisol levels and age, neither in the CHD group nor in the control group. However, children with CHD had overall higher cortisol levels than healthy controls (Figure 7 A). This difference in cortisol levels was more evident in the younger age groups, and particularly in children younger than 1 month of age, corresponding to severe CHD (Figure 7 B). These data indicate that CHD might influence the T cell development in the thymus due to high cortisol levels, and that the severity of the heart disease might further affect the composition of developing thymocytes.

2.4 DISCUSSION AND PERSPECTIVES

2.4.1 A multicolour flow cytometry panel to analyse T cell development

During my doctoral thesis, I have designed and tested a staining panel to evaluate human T cell development in the thymus that allows a clear definition of the main thymocyte subsets ranging from progenitors that just entered the thymus to mature thymocytes that are ready to egress to the periphery. The analysis of all subsets in one tube facilitates statistical analysis and the visualisation of multi-dimensional data. Using this panel on donors between 6 and 12 months of age without known genetic syndromes, we provide reference values for the frequencies of thymocyte subsets at all stages of development. Here, it is important to keep in mind that frequencies will change in other age groups (17,52) and in children with syndromes affecting the immune system, such as Down syndrome (DS) or DiGeorge syndrome (53–57), and would most likely differ in children without CHD. Samples from the latter are not easily available.

2.4.2 Glucocorticoids cause thymocyte apoptosis at specific stages of development

Administration of prenatal GCs is associated with impaired foetal thymic growth (33,34). GCs cause apoptosis in thymocytes, predominantly in the DP compartment (58). We used our comprehensive T cell development panel to further elucidate which are the most GC-susceptible subpopulations. We found that not only the DP thymocytes die, but also the more immature CD45low CD34+ cells, in particular ISP4 CD34+ cells. A possible mechanistic explanation for GC-induced apoptosis in DP cells is the GC-induced downregulation of genes promoting thymocyte survival like *Notch1* and the upregulation of genes with pro-apoptotic function (59). Additionally, we identified surface markers that are associated with an increased risk for GC-induced apoptosis or with a survival advantage of the thymocytes. CD28, which marks ß-selection in human thymocytes (11) and is upregulated in a fraction of ISP4 CD34- cells (1), is already described as a mediator of GC-resistance in thymocytes (60). Not all surface marker functions are fully understood, and it will be interesting to further elucidate their role in T cell development and how they affect sensitivity to GCs. A better understanding of the pathways that induce lung maturation and those that induce thymocyte apoptosis could pave the way for the application of synthetic GR ligands that selectively modulate the GR and promote the desired molecular actions while reducing side effects (selective GR modulators or agonists are reviewed in (61–63)).

2.4.3 Challenges of modelling T cell development *in vitro*

In the OP9 model for *in vitro* T cell development, we could follow the generation of DP as well as CD4 and CD8 SP thymocytes, and could show proliferation impairment and delayed development in thymocytes that had received a pulse of betamethasone. However, there are some limitations that need to be considered when interpreting data obtained with this system. OP9 cocultures lasting up to 49 days are described in literature (64). Possible causes for the shorter lifetime of our cultures are the use of CD34+ thymocytes that are more differentiated compared to stem cells isolated from cord blood. OP9 cells present a limited number of self-antigens and do not express MHC class II molecules and therefore, do not sufficiently support selection processes (49). We observed deviations from *in vivo* human T cell development and simplified the gating strategy presented in OMIP 073 accordingly to focus on the main compartments (DN, DP, CD4+ and CD8+). T cell development *in vitro* displayed a high biological variability that was probably caused by the heterogeneous group of samples used in the cultures (broad age range and one sample with DS). To improve significance, experiments could be repeated with a larger sample size and a homogenous group of samples. Recently, we established the generation of T cells in artificial thymic organoids (ATOs) in our lab. These three-dimensional systems show improved selection processes and reduced inter-assay variability, probably due to the use of serum-free medium (65). We could optimise the lifetime of the ATOs by adding SCF only in the first week of culture. Further investigations using ATOs will extend our knowledge about the effects of short-term betamethasone exposure on T cell development and will help to understand the consequences of prenatal GC treatment on the development of the immune system.

2.4.4 Does congenital heart disease affect the T cell development in children?

CHD affects approximately 1 % of all live births. In Germany, about 8500 children are born with CHD each year and about one third of them needs to undergo surgery within the first year of life (66). Knowledge on the immunological consequences of thymectomy increases steadily (67–70), but little is known about the influence of CHD *per se* on thymus size and T cell development. Since patients with CHD are at higher risk for severe infections, it is important to consider a latent immune deficiency (71). In the last few years, whole genome and exome sequencing techniques have revealed ~400 genes associated to the pathogenesis of CHD (72). Interestingly, mutations that cause dysregulation of heart development were found in signalling pathways that are essential for proper T cell development. A remarkable example is *NOTCH1* regulating valve formation (72,73) and also required for T lineage commitment (74). Newborns with CHD present with lower TREC levels than controls, and an association of decreased TREC levels and hospitalisation due to infection is reported for preterm children with CHD (75).

We observed an increase of the DP frequencies and a decrease of the SP frequencies with age, previously described as “transient thymic involution” (17,52). Children with the most severe CHD had lower DP frequencies and higher SP frequencies, indicating that neonates with CHD might suffer from a relatively higher cortisol burden, even though it is not known if the thymus of neonates exhibits the same sensitivity to increased cortisol levels than the thymus of older infants. This raises the question if the transient thymic involution is a completely physiological process that is exclusively caused by age and in response to physiologically increased GC-levels during late gestation (52,76) or if the consequences of severe CHD (high cortisol levels or cyanosis) are responsible for the described

changes. The ideal samples to clarify this question would be thymic tissue from children without CHD, but there are only rare cases of thoracic surgery in children without heart disease.

Elucidating the impact of CHD on T cell development would help to understand the immunological challenges in the lives of children with CHD and could contribute to improve prevention, diagnosis and treatment of comorbidities, underlining the need for further research on this topic.

3 SUMMARY

3.1 ENGLISH

Introduction: The thymus provides the microenvironment for T cell development and enables the generation of a broad repertoire of functional and self-tolerant T cells. We hypothesise that impairment of thymic function during early life increases the risk of developing immune-mediated disorders later in life. The aim of this thesis is to establish a flow cytometry panel that allows a comprehensive *ex vivo* and *in vitro* assessment of T cell development in different health conditions and under exposure to exogenous insults such as medication.

Methods: We designed a multicolour flow cytometry panel that allows us to phenotype the stages of T cell development on the basis of surface marker expression. The panel was thoroughly optimized, including titration, compensation and the comparison of a variety of fluorochrome-conjugated antibody combinations. We used the panel to investigate the effects of glucocorticoids (GCs) on developing thymocytes. For this, we used an *in vitro* assay to determine the sensitivity of the different human thymocyte populations to betamethasone, and the OP9 coculture system to model T cell development *in vitro* and analyse how GCs affect the dynamics of lymphopoiesis. Second, we immune phenotyped the thymi of 44 infants with CHD and compared the "thymocyte signatures" among age groups and different types of CHD.

Results: With the established panel we have identified the major stages of human T cell development, from early progenitors to mature T cells ready to egress the thymus. We observed that *in vitro* betamethasone exposure induced apoptosis in thymocytes, mainly affecting the immature CD4 single-positive CD34-positive (ISP4 CD34+) and the double-positive (DP) population, leading to a relative increase of T regulatory, CD4 and CD8 single-positive (SP) cells. Furthermore, GCs caused a delayed thymocyte development in the OP9 coculture system. Children with CHD had higher cortisol levels than healthy controls, so their thymocyte composition is most likely influenced by endogenous GC exposure. We found a specific thymocyte signature in the most severe CHD groups (transposition of the great arteries and a group summarised as "left hypoplasia") with decreased DP frequencies and concomitantly increased CD4 SP frequencies. Additionally, we found correlations between reduced DP frequencies and young age (< 1 month) and elevated cardiac biomarkers, respectively.

Conclusion: The established panel proved to be a reliable tool to analyse T cell development *ex vivo* and *in vitro*. We have acquired valuable knowledge on the effects of GCs on specific thymocyte subpopulations with data from *in vitro* modelling of T cell development. Finally, our *ex vivo* data suggest a possible influence of CHD on T cell development and indicate that CHD itself might cause immune alterations.

3.2 DEUTSCH

Einleitung: Der Thymus ist ein spezialisiertes lymphatisches Gewebe und dient als Entwicklungsnische für T-Zellen. Diese durchlaufen eine Reihe von Selektionsprozessen und bilden schließlich ein umfangreiches, selbsttolerantes Repertoire. Wir nehmen an, dass Störungen der T-Zell-Entwicklung im Thymus während der frühkindlichen Entwicklung zu immunologischen Erkrankungen führen können. Das Ziel dieser Dissertationsarbeit ist es, ein Panel zur differenzierten durchflusszytometrischen Analyse von Thymozyten zu entwickeln. Dieses soll neue Einblicke in die T-Zell-Entwicklung bei verschiedenen Erkrankungen und unter äußeren Einflussfaktoren, wie bspw. Medikation, ermöglichen.

Methoden: Wir entwickelten und optimierten ein FACS-Panel zur Phänotypisierung von Thymozyten anhand der Expression verschiedener Oberflächenmarker. Mithilfe dieses Panels untersuchten wir zunächst den Effekt von Glukokortikoiden auf sich entwickelnde Thymozyten. Hierfür nutzen wir ein *in vitro*-Assay, um die Glukokortikoidsensitivität der unterschiedlichen Thymozyten-Populationen zu ermitteln, sowie die OP9-Kokultur als *in vitro*-Modell für T-Zell-Entwicklung, um den Effekt von Glukokortikoiden auf die Entwicklungsdynamik der Thymozyten zu analysieren. Zusätzlich immunophänotypisierten wir die Thymi von 44 Kleinkindern (Alter <1 Jahr) mit angeborenen Herzfehlern und verglichen die Immunsignaturen zwischen den Altersgruppen und zwischen den verschiedenen Arten von Herzfehlern.

Ergebnisse: Mithilfe des neu entwickelten Panels konnten die wesentlichen Thymozyten-Subpopulationen definiert werden, von frühen Vorläuferzellen bis zu vollständig gereiften, einfach-positiven T-Zellen, die in die Peripherie migrieren können. Wir beobachteten, dass Betamethasonexposition *in vitro* Apoptose in insbesondere den CD4-positiven CD34-positiven sowie den CD4-CD8-doppelt-positiven Thymozyten auslöste und es hierdurch zu einem relativen Anstieg der CD4- und CD8-einfach-positiven Thymozytenpopulationen kam. In der OP9-Kokultur kam es nach Betamethasonexposition zu einer Entwicklungsverzögerung der Thymozyten. Da wir zeigen konnten, dass Kinder mit angeborenen Herzfehlern im Vergleich zur Kontrollgruppe erhöhte Kortisolwerte aufweisen, gehen wir davon aus, dass deren Thymozytenentwicklung durch die endogen erhöhten Kortisolwerte beeinflusst wird. In den Gruppen mit den schwersten Herzfehlern (Transposition der großen Arterien und Hypoplastisches Linksherzsyndrom/ Aortenstenose/ Unterbrochener Aortenbogen) zeigte sich eine veränderte Komposition der Thymozytenpopulationen mit einer prozentual verminderten doppelt-positiven Population und einem kompensatorisch erhöhten Anteil an CD4-einfach-positiven Thymozyten. Zudem fanden wir Korrelationen zwischen einer verminderten doppelt-positiven Population und jungem Alter (< 1 Monat) bzw. erhöhten kardialen Markern wie Troponin T und NT-proBNP.

Schlussfolgerung: Das etablierte Panel konnte verlässlich zur Analyse der T-Zell-Entwicklung *ex vivo* und *in vitro* eingesetzt werden und mithilfe des Panels konnten wir bereits vorbestehendes Wissen über den Einfluss von Glukokortikoiden auf Thymozyten mit Daten zur Entwicklungsdynamik erweitern. Des Weiteren lassen unsere *ex vivo* Daten einen möglichen Einfluss von angeborenen Herzfehlern auf die Zusammensetzung der Thymozytenpopulationen erkennen und weisen darauf hin, dass angeborene Herzfehler zu Veränderungen des Immunsystem führen können.

4 TABLES AND FIGURES

4.1 TABLE 1

		Cohort (n=44)
Age (days)		mean: 132, min: 2, max: 363
Gender		female: 14 (32 %), male: 30 (68 %)
Heart disease (leading diagnosis)	VSD	11 (25 %) mean age (days): 196
	ToF	4 (9 %) mean age (days): 183
	TGA	9 (20 %) mean age (days): 11
	AVSD	8 (18 %) mean age (days): 166
	ASD	4 (9 %) mean age (days): 239
	"left hypoplasia"	6 (14 %) mean age (days): 26
	Others	2 (5 %) mean age (days): 202
NT-proBNP (ng/l)		mean: 10659, min: 115, max: 66721
Troponin T (pg/ml) (n=28)		mean: 47.25, min: 7, max: 217

Table 1. Characteristics of the study population.

Abbreviations: VSD: Ventricular septal defect, ToF: Tetralogy of Fallot, TGA: Transposition of the great arteries, AVSD: Atrioventricular septal defect, ASD: Atrial septal defect, "left hypoplasia": Hypoplastic left heart syndrome or Aortic stenosis / Interrupted aortic arch

4.2 FIGURE 1

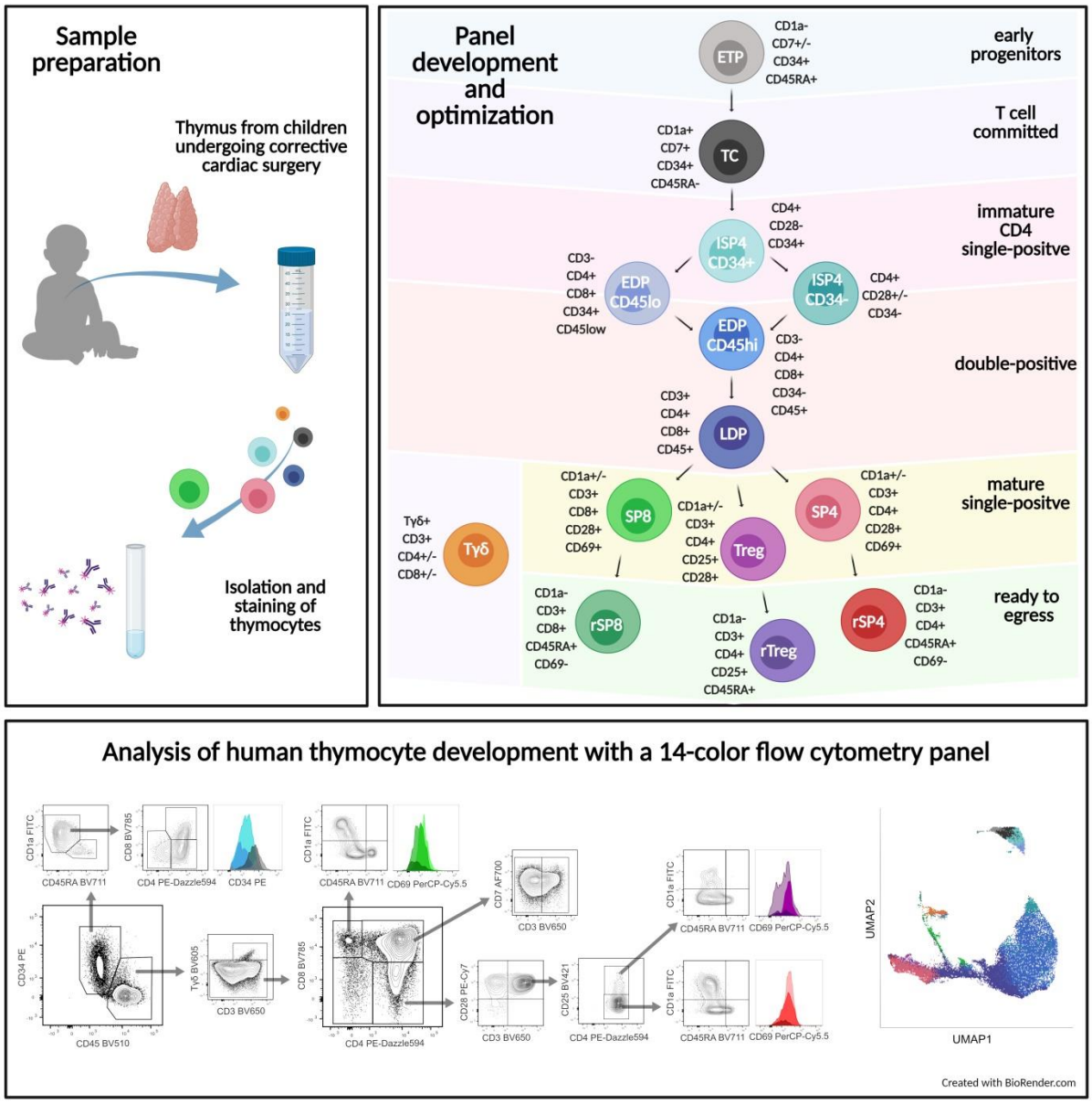

Figure 1. Establishment of an "Optimized Multicolor Immunofluorescence Panel" for the analysis of human T cell development. Graphical abstract of Bremer et al. 2021 (1).

4.3 FIGURE 2

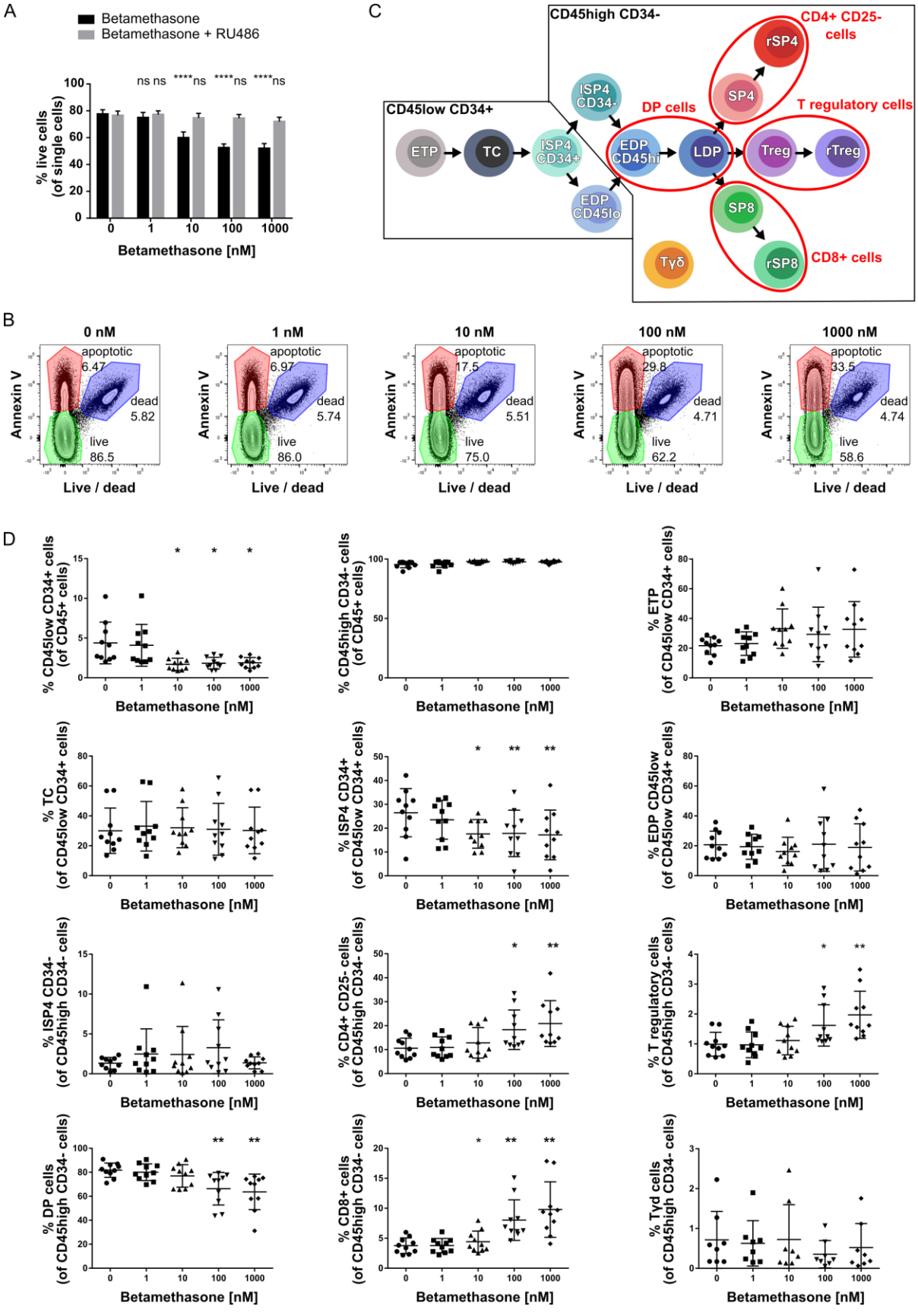
A
Betamethasone
Betamethasone + RU486
% live cells (of single cells)
ns ns ****ns ****ns ****ns
Betamethasone [nM]
C
CD45high CD34-
CD4+ CD25- cells
rSP4
SP4
ISP4 CD34-
DP cells
T regulatory cells
CD45low CD34+
ETP
TC
ISP4 CD34+
EDP CD45hi
LDP
Treg
rTreg
EDP CD45lo
SP8
Tγδ
rSP8
CD8+ cells
B
0 nM
1 nM
10 nM
100 nM
1000 nM
Annexin V
apoptotic 6.47
dead 5.82
live 86.5
apoptotic 6.97
dead 5.74
live 86.0
apoptotic 17.5
dead 5.51
live 75.0
apoptotic 29.8
dead 4.71
live 62.2
apoptotic 33.5
dead 4.74
live 58.6
Live / dead
D
% CD45low CD34+ cells (of CD45+ cells)
% CD45high CD34- cells (of CD45+ cells)
% ETP (of CD45low CD34+ cells)
% TC (of CD45low CD34+ cells)
% ISP4 CD34+ (of CD45low CD34+ cells)
% EDP CD45low (of CD45low CD34+ cells)
% ISP4 CD34- (of CD45high CD34- cells)
% CD4+ CD25- cells (of CD45high CD34- cells)
% T regulatory cells (of CD45high CD34- cells)
% DP cells (of CD45high CD34- cells)
% CD8+ cells (of CD45high CD34- cells)
% Tγd cells (of CD45high CD34- cells)
Betamethasone [nM]

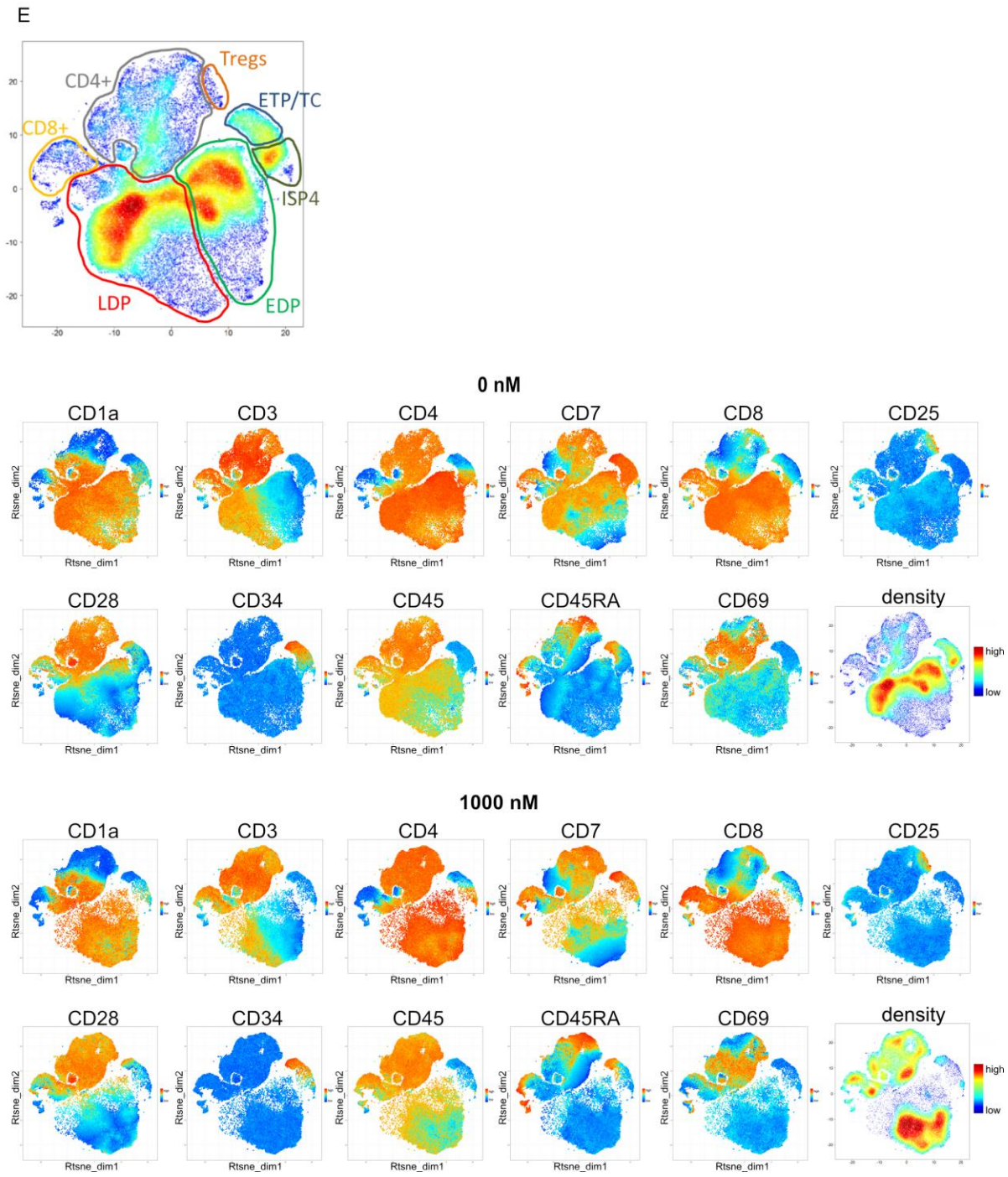

Figure 2. *In vitro* effect of betamethasone on thymocyte subsets. (A) Frequencies of live cells out of single cells after overnight incubation. Thymocytes were incubated for 16 hours with increasing concentrations of betamethasone (black bars) and with betamethasone in combination with RU-486 (grey bars), respectively. n=7 per group. Statistical analysis was performed with Bonferroni's multiple comparisons test by comparing each group (1 nM, 10 nM, 100 nM, 1000 nM) to control (0 nM). (B) Representative FACS plots of thymocytes after incubation with increasing concentrations of betamethasone without RU-486 as shown in (A). Live cells are shown in green, apoptotic cells in red and dead cells in blue. Frequencies of populations out of single cells are indicated. (C) Scheme of T cell development in the thymus. Populations that are summarised for analysis are indicated. (D) Frequencies of thymocyte subsets after overnight incubation with increasing concentrations of betamethasone. n=10. Thymi with < 60 % of DP cells (out of CD45high CD34-) were excluded from

analysis. Statistical analysis was performed with Bonferroni's multiple comparisons test by comparing each group to control. Significance is indicated if it reaches $p < 0.05$. (E) t-SNE plots visualizing the expression of individual thymocyte surface markers as well as cell density. Only live, CD45+ cells are depicted and each dot represents one cell. In the first plot, the major populations are encircled. Below, the two upper rows show a representative sample after incubation with 0 nM betamethasone, the lower rows show a sample from the same donor after incubation of thymocytes with 1000 nM betamethasone. Compensated FCS files were exported from FlowJo and analysed in R (analysis in R was performed by Laura Glau). ns $p \geq 0.05$, * $p < 0.05$, ** $p < 0.01$, *** $p < 0.001$, **** $p < 0.0001$.

4.4 FIGURE 3

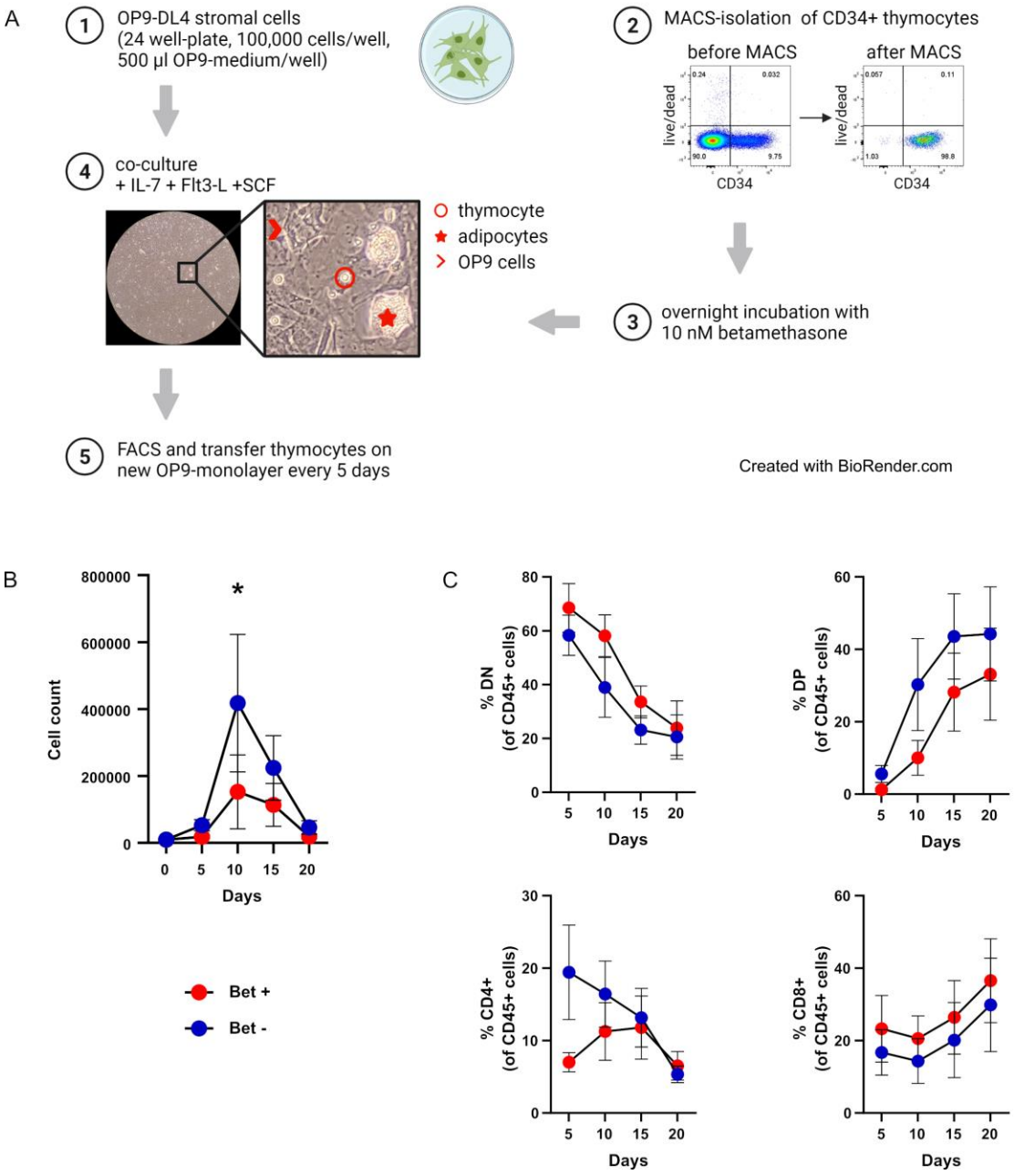

Figure 3. Effects of betamethasone on the T cell development in the OP9 coculture system. (A) Schematic workflow for OP9 coculture system. (B) Development of cell counts after 0 to 20 days of coculture with (shown in red) or without (shown in blue) pre-incubation with betamethasone. Day 0 to 15: n=6 per group, day 20: n=5 per group. Multiple t tests were performed for statistical analysis. (C) Development of thymocyte populations after 5 to 20 days of culture. Depicted populations were gated out of single cells, live cells, CD45+ cells. Day 5 to 15: n=6 per group, day 20 n=5 per group. Depicted is the mean with standard error. * $p < 0.05$, ** $p < 0.01$, *** $p < 0.001$, **** $p < 0.0001$

4.5 FIGURE 4

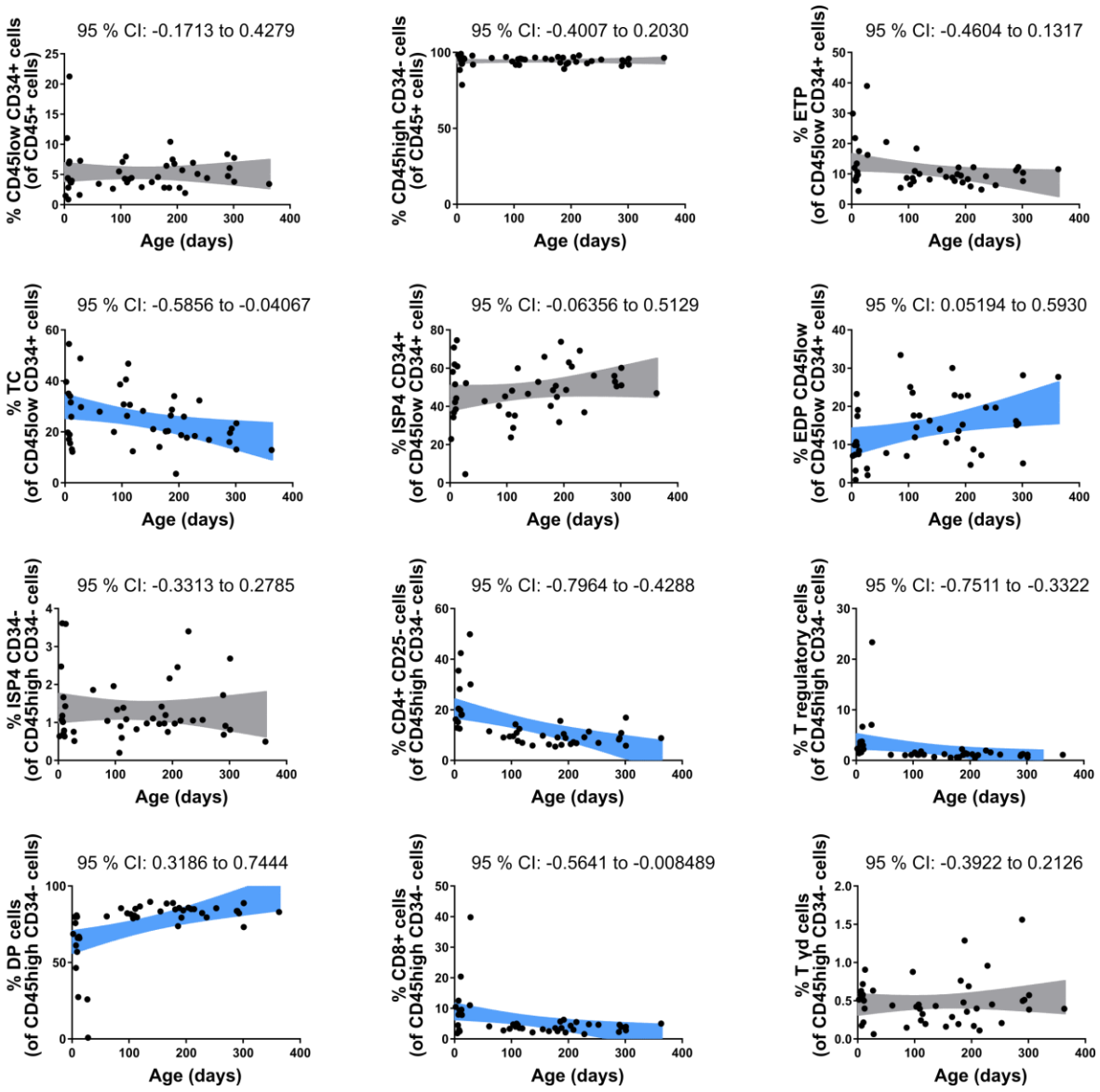

Figure 4. Thymocyte subsets in the context of age. Frequencies of thymocyte subpopulations in children with CHD aged 2 to 363 days. Data were obtained from the cohort presented in Table 1 (n=44). For statistical analysis, correlation was calculated with Spearman r. The 95 % confidence interval (CI) of linear regression analysis is depicted in colour and indicated in the plot. For confidence intervals depicted in grey, two-tailed t test achieved no significance; for confidence intervals depicted in blue, two-tailed t test revealed significance with $p < 0.05$.

4.6 FIGURE 5

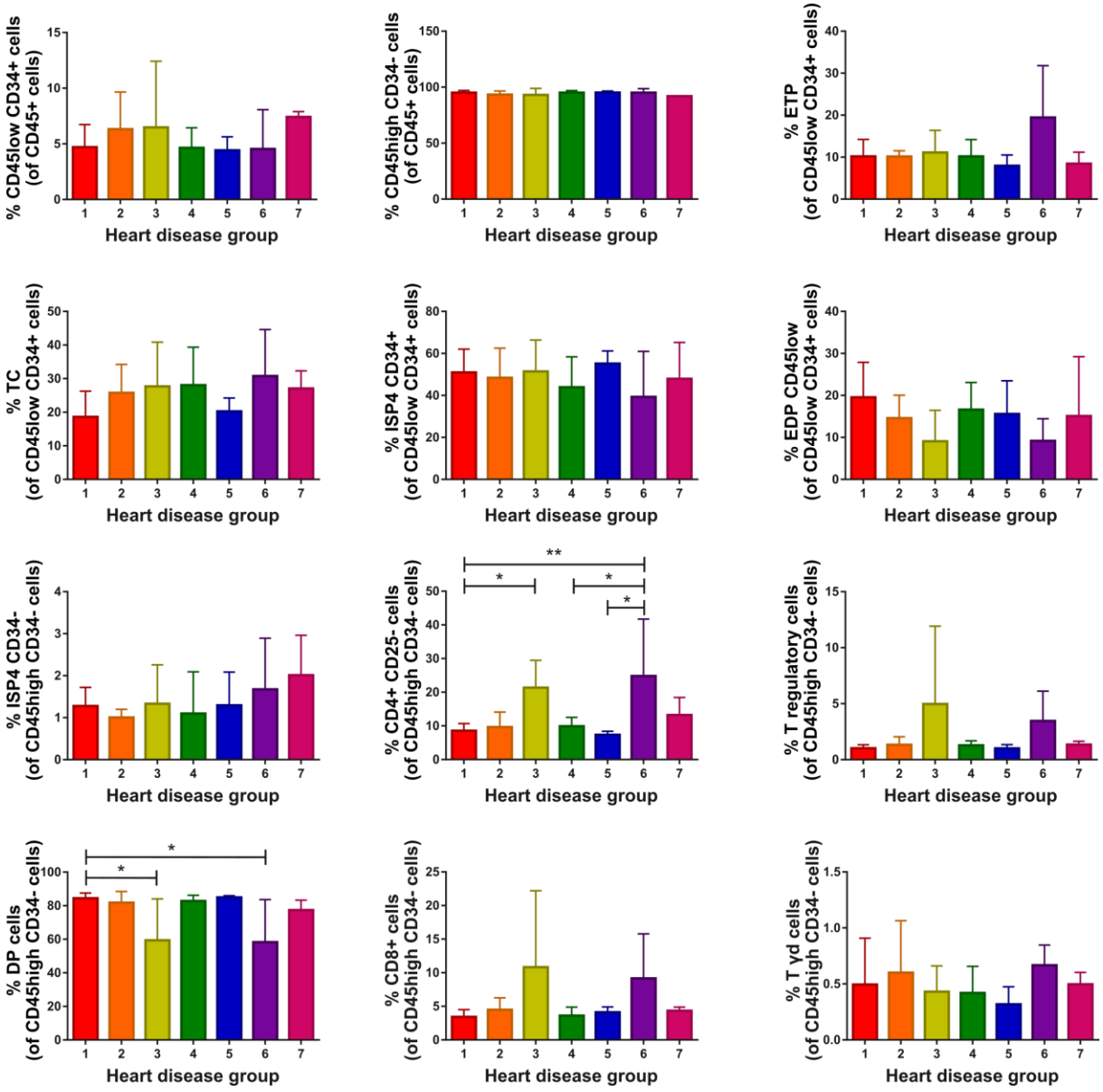

Figure 5. Thymocyte subsets in the context of heart disease. Frequencies of thymocyte subpopulations in children with CHD with following diseases: 1 VSD (n=11), 2 ToF (n=4), 3 TGA (n=9), 4 AVSD (n=8), 5 ASD (n=4), 6 “left hypoplasia” (n=6), 7 others (n=2). Data were obtained from the cohort presented in Table 1 (n=44). The plots show the mean with standard deviation. Statistical analysis was performed with One-Way-ANOVA and Bonferroni correction and is indicated in case of significance. * $p < 0.05$, ** $p < 0.01$, *** $p < 0.001$, **** $p < 0.0001$

4.7 FIGURE 6

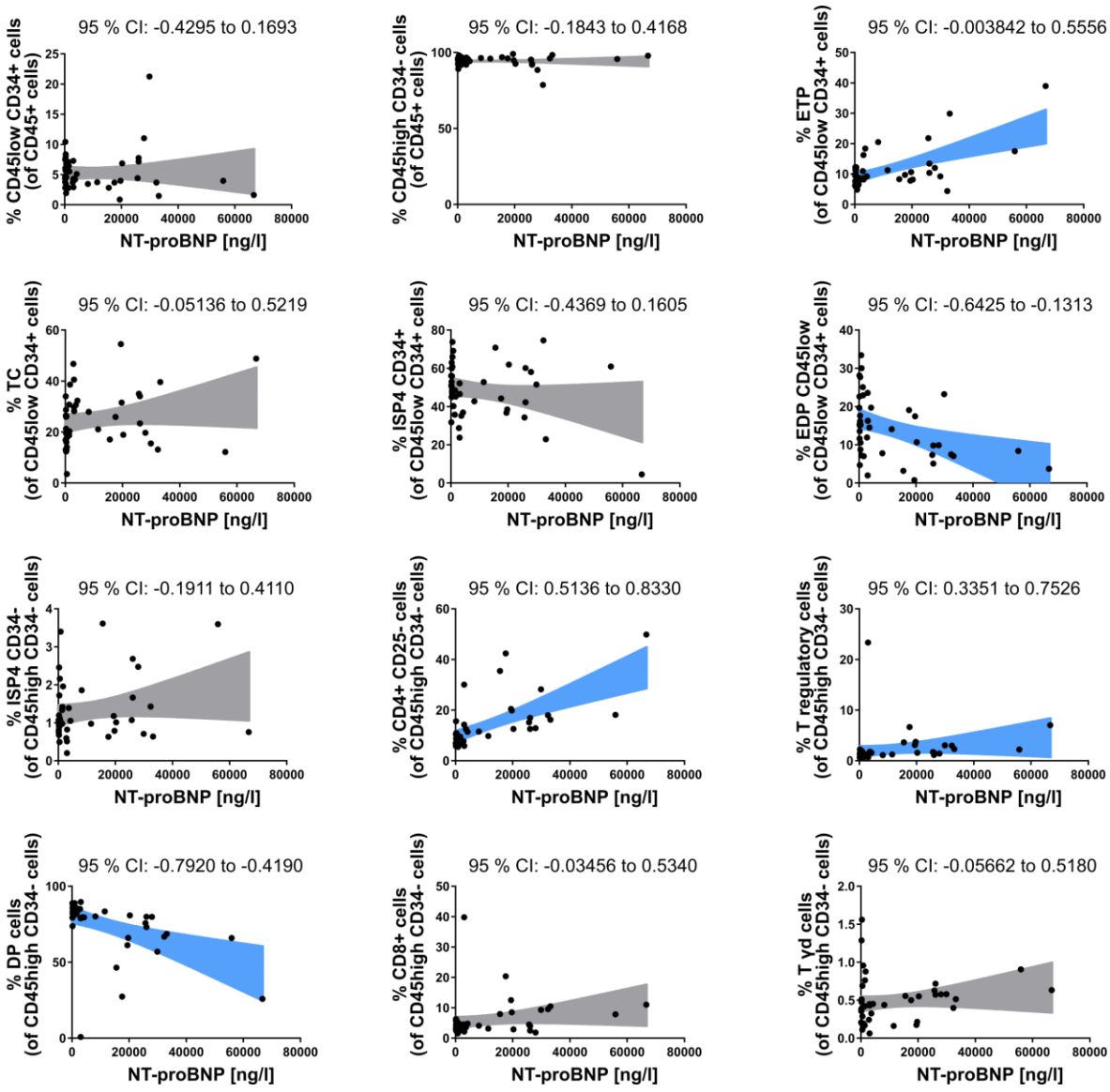

Figure 6. Correlation of thymocyte subsets with NT-proBNP. Frequencies of thymocyte subpopulations in children with CHD are correlated to preoperative levels of NT-proBNP. Data were obtained from the cohort presented in Table 1 (n=44). For statistical analysis, correlation was calculated with Spearman r. The 95 % confidence interval (CI) of linear regression analysis is depicted in colour and indicated in the plot. For confidence intervals depicted in grey, two-tailed t test achieved no significance; for confidence intervals depicted in blue, two-tailed t test revealed significance with $p < 0.05$.

4.8 FIGURE 7

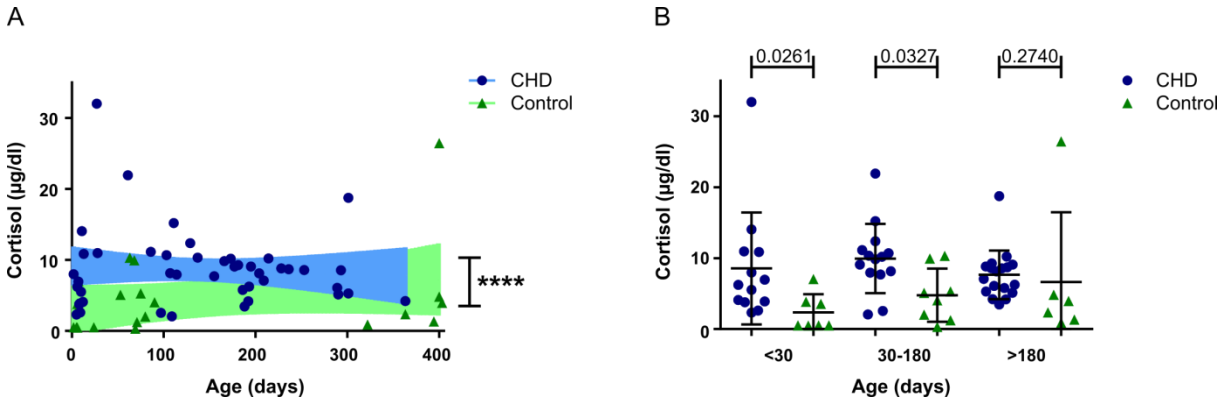

Figure 7. Plasma cortisol concentrations of children with CHD (blue) (n=45) and healthy controls (green) (n=21). One sample that was above measurement threshold was included with a cortisol level of 32 µg/dl, and three samples that were below measurement threshold were included with cortisol levels of 0.5 µg/dl. (A) Linear regression and Spearman correlation were calculated: 95% confidence intervals depicted in colour: CHD: -0.2335 to 0.3669, Control: -0.1528 to 0.6625. Groups (CHD and Control) were compared with Mann Whitney test. (B) Comparison of cortisol levels in children with CHD and controls within three age groups. For statistical analysis, Kruskal-Wallis test was performed with Dunn's correction for multiple comparisons. Adjusted p values are indicated above columns. ns $p \geq 0.05$, * $p < 0.05$, ** $p < 0.01$, *** $p < 0.001$, **** $p < 0.0001$.

5 REFERENCES

1. Bremer S-J, Glau L, Gehbauer C, Boxnick A, Biermann D, Sachweh JS, et al. OMIP 073 : Analysis of human thymocyte development with a 14-color flow cytometry panel. Cytom Part A. 2021;1–5.
2. Miller JFAP. Immunological Function of the Thymus. Lancet. 1961;278(7205):748–9.
3. Miller JFAP, Mitchell GF. The thymus and the precursors of antigen reactive cells. Nature. 1967;216(5116):659–63.
4. Miller J. The early work on the discovery of the function of the thymus, an interview with Jacques Miller. Cell Death Differ. 2020;27(1):396–401.
5. Lind EF, Prockop SE, Porritt HE, Petrie HT. Mapping precursor movement through the postnatal thymus reveals specific microenvironments supporting defined stages of early lymphoid development. J Exp Med. 2001;194(2):127–34.
6. Terstappen LWMM, Huang S, Picker LJ. Flow Cytometric Assessment of Human T-Cell Differentiation in Thymus and Bone Marrow. Blood. 1992;79(3):666–77.
7. Canté-Barrett K, Mendes RD, Li Y, Vroegindeweij E, Pike-Overzet K, Wabeke T, et al. Loss of CD44dim expression from early progenitor cells marks T-cell lineage commitment in the human thymus. Front Immunol. 2017;8(32).
8. Lavaert M, Liang KL, Vandamme N, Park J-E, Roels J, Kowalczyk MS, et al. Integrated scRNA-Seq Identifies Human Postnatal Thymus Seeding Progenitors and Regulatory Dynamics of Differentiating Immature Thymocytes. Immunity. 2020;52:1–17.
9. Dik WA, Pike-Overzet K, Weerkamp F, de Ridder D, de Haas EFE, Baert MRM, et al. New insights on human T cell development by quantitative T cell receptor gene rearrangement studies and gene expression profiling. J Exp Med. 2005;201(11):1715–23.
10. Spits H. Development of αβ T cells in the human thymus. Nat Rev Immunol. 2002;2(10):760–72.
11. Taghon T, Van de Walle I, De Smet G, De Smedt M, Leclercq G, Vandekerckhove B, et al. Notch signaling is required for proliferation but not for differentiation at a well-defined beta-selection checkpoint during human T-cell development. Blood. 2009;113(14):3254–63.
12. Klein L, Kyewski B, Allen PM, Hogquist KA. Positive and negative selection of the T cell repertoire: What thymocytes see (and don't see). Nat Rev Immunol. 2014;14(6):377–91.
13. Karimi MM, Guo Y, Cui X, Pallikonda HA, Horková V, Wang YF, et al. The order and logic of CD4 versus CD8 lineage choice and differentiation in mouse thymus. Nat Commun. 2021;12(1):1–14.
14. Plum J, De Smedt M, Leclercq G, Taghon T, Kerre T, Vandekerckhove B. Human intrathymic development: A selective approach. Semin Immunopathol. 2008;30(4):411–23.
15. Lobach DF, Hensley LL, Ho W, Haynes BF. Human T cell antigen expression during the early stages of fetal thymic maturation. J Immunol. 1985;135(3):1752–9.
16. George AJT, Ritter MA. Thymic involution with ageing: obsolescence or good housekeeping? Immunol Today. 1996;17(6):267–72.
17. Weerkamp F, De Haas EFE, Naber BAE, Comans-Bitter WM, Bogers AJJC, Van Dongen JJM, et al. Age-related changes in the cellular composition of the thymus in children. J Allergy Clin

Immunol. 2005;115(4):834–40.

18. Haynes BF, Markert ML, Sempowski GD, Patel DD, Hale LP. The Role of the Thymus in Immune Reconstitution in Aging, Bone Marrow Transplantation, and HIV-1 Infection. Annu Rev Immunol. 2000;18:529–60.
19. Douek DC, McFarland RD, Keiser PH, Gage EA, Massey JM, Haynes BF, et al. Changes in thymic function with age and during the treatment of HIV infection. Nature. 1998;396(6712):690–5.
20. Galon J, Franchimont D, Hiroi N, Frey G, Boettner A, Ehrhart-Bornstein M, et al. Gene profiling reveals unknown enhancing and suppressive actions of glucocorticoids on immune cells. FASEB J. 2002;16(1):61–71.
21. Cain DW, Cidlowski JA. Immune regulation by glucocorticoids. Nat Rev Immunol. 2017;17(4):233–47.
22. Wyllie AH. Glucocorticoid-induced thymocyte apoptosis is associated with endogenous endonuclease activation. Nature. 1980;284(5756):555–6.
23. Solano ME, Holmes MC, Mittelstadt PR, Chapman KE, Tolosa E. Antenatal endogenous and exogenous glucocorticoids and their impact on immune ontogeny and long-term immunity. Semin Immunopathol. 2016;38(6):739–63.
24. Mittelstadt PR, Taves MD, Ashwell JD. Cutting Edge: De Novo Glucocorticoid Synthesis by Thymic Epithelial Cells Regulates Antigen-Specific Thymocyte Selection. J Immunol. 2018;200:1988–94.
25. Jan Wiegers G, Knoflach M, Böck G, Niederegger H, Dietrich H, Falus A, et al. CD4+CD8+TCRlow thymocytes express low levels of glucocorticoid receptors while being sensitive to glucocorticoid-induced apoptosis. Eur J Immunol. 2001;31(8):2293–301.
26. Bouillet P, Purton JF, Godfrey DI, Zhang LC, Coultas L, Puthalakath H, et al. BH3-only Bcl-2 family member Bim is required for apoptosis of autoreactive thymocytes. Nature. 2002;415(6874):922–6.
27. Erlacher M, Labi V, Manzl C, Böck G, Tzankov A, Häcker G, et al. Puma cooperates with Bim, the rate-limiting BH3-only protein in cell death during lymphocyte development, in apoptosis induction. J Exp Med. 2006;203(13):2939–51.
28. Taves MD, Ashwell JD. Glucocorticoids in T cell development, differentiation and function. Nat Rev Immunol. 2021;21(4):233–43.
29. Mittelstadt PR, Taves MD, Ashwell JD. Glucocorticoids oppose thymocyte negative selection by inhibiting Helios and Nur77. J Immunol. 2019;203(8):2163–70.
30. Taves MD, Mittelstadt PR, Presman DM, Hager GL, Ashwell JD. Single-Cell Resolution and Quantitation of Targeted Glucocorticoid Delivery in the Thymus. 2019;26(13):3629–42.
31. Roberts D, Brown J, Medley N, Dalziel S. Antenatal corticosteroids for accelerating fetal lung maturation for women at risk of preterm birth (Review). Cochrane Database Syst Rev. 2017;1(3):1–273.
32. WHO. WHO Recommendations on Interventions to Improve Preterm Birth Outcomes. WHO Recommendations on Interventions to Improve Preterm Birth Outcomes. 2015. p. 98.
33. Jones CA, Nisenbaum R, De Souza LR, Berger H. Antenatal corticosteroid administration is associated with decreased growth of the fetal thymus: a prospective cohort study. J Perinatol. 2020;40(1):30–8.

34. Michie C, Hasson N, Tulloh R. The neonatal thymus and antenatal steroids. Arch Dis Child Fetal Neonatal. 1998;79(F0):159.
35. Palojärvi A, Andersson S, Turpeinen U, Janér C, Petäjä J. Antenatal betamethasone associates with transient immunodepression in very low birth weight infants. Neonatology. 2013;104(4):275–82.
36. Vermillion ST, Soper DE, Newman RB. Neonatal sepsis and death after multiple courses of antenatal betamethasone therapy. Am J Obstet Gynecol. 2000;183(4):810–4.
37. Pole JD, Mustard CA, To T, Beyene J, Allen AC. Antenatal steroid therapy for fetal lung maturation: Is there an association with childhood asthma? J Asthma. 2009;46(1):47–52.
38. Greene NH, Pedersen LH, Liu S, Olsen J. Prenatal prescription corticosteroids and offspring diabetes: A national cohort study. Int J Epidemiol. 2013;42(1):186–93.
39. Hong JY, Lim J, Carvalho F, Cho JY, Vaidyanathan B, Yu S, et al. Long-term programming of CD8 T cell immunity by perinatal exposure to glucocorticoids. Cell. 2020;180(5):847–61.
40. Diepenbruck I, Much CC, Krumbholz A, Kolster M, Thieme R, Thieme D, et al. Effect of prenatal steroid treatment on the developing immune system. J Mol Med. 2013;91(11):1293–302.
41. Gieras A, Gehbauer C, Perna-Barrull D, Engler JB, Diepenbruck I, Glau L, et al. Prenatal administration of betamethasone causes changes in the T cell receptor repertoire influencing development of autoimmunity. Front Immunol. 2017;8(1505):1–15.
42. Raff H, Lee JJ, Widmaier EP, Oaks MK, Engeland WC. Basal and Adrenocorticotropin-Stimulated Corticosterone in the Neonatal Rat Exposed to Hypoxia from Birth: Modulation by Chemical Sympathectomy. Endocrinology. 2004;145(1):79–86.
43. Zayour D, Azar ST, Azar N, Nasser M, Obeid M, Mroueh S, et al. Endocrine changes in a rat model of chronic hypoxia mimicking cyanotic heart disease. Endocr Res. 2003;29(2):191–200.
44. Kodama T, Shimizu N, Yoshikawa N, Makino Y, Ouchida R, Okamoto K, et al. Role of the glucocorticoid receptor for regulation of hypoxia-dependent gene expression. J Biol Chem. 2003;278(35):33384–91.
45. Li L, Bahtiyar MO, Buhimschi CS, Zou L, Zhou QC, Copel JA. Assessment of the fetal thymus by two- and three-dimensional ultrasound during normal human gestation and in fetuses with congenital heart defects. Ultrasound Obstet Gynecol. 2011;37(4):404–9.
46. Caprirolo G, Ghanayem NS, Murkowski K, Nugent ML, Simpson PM, Raff H. Circadian rhythm of salivary cortisol in infants with congenital heart disease. Endocrine. 2013;43(1):214–8.
47. Gul KA, Strand J, Pettersen RD, Brun H, Abrahamsen TG. T-cell Receptor Excision Circles in Newborns with Heart Defects. Pediatr Cardiol. 2020;41(4):809–15.
48. Mahnke Y, Chattopadhyay P, Roederer M. Publication of Optimized Multicolor Immunofluorescence Panels. Cytom Part A. 2010;77A(9):814–8.
49. Zúñiga-Pflücker J. T-cell development made simple. Nat Rev Immunol. 2004;4(1):67–72.
50. McKie PM, Burnett JC. NT-proBNP: The Gold Standard Biomarker in Heart Failure. J Am Coll Cardiol. 2016;68(22):2437–9.
51. Lipshultz SE, Rifai N, Sallan SE, Lipsitz SR, Dalton V, Sacks DB, et al. Predictive value of cardiac troponin T in pediatric patients at risk for myocardial injury. Circulation. 1997;96(8):2641–8.
52. Varas A, Jimenez E, Sacedon R, Rodriguez-Mahou M, Maroto E, Zapata AG, et al. Analysis of

the Human Neonatal Thymus: Evidence for a Transient Thymic Involution. J Immunol. 2000;164:6260–7.

53. Levin S, Schlesinger M, Handzel Z, Hahn T, Altman Y, Czernobilsky B, et al. Thymic Deficiency in Down's Syndrome. Pediatrics. 1979;63(1):80–7.
54. Murphy M, Lempert MJ, Epstein LB. Decreased level of T cell receptor expression by Down syndrome (trisomy 21) thymocytes. Am J Med Genet Suppl. 1990;7:234–7.
55. Skogberg G, Lundberg V, Lindgren S, Gudmundsdottir J, Sandström K, Kämpe O, et al. Altered Expression of Autoimmune Regulator in Infant Down Syndrome Thymus, a Possible Contributor to an Autoimmune Phenotype. J Immunol. 2014;193(13):2187–95.
56. Marcovecchio GE, Bortolomai I, Ferrua F, Fontana E, Imberti L, Conforti E, et al. Thymic Epithelium Abnormalities in DiGeorge and Down Syndrome Patients Contribute to Dysregulation in T Cell Development. Front Immunol. 2019;10(447):1–15.
57. Marcovecchio GE, Ferrua F, Fontana E, Beretta S, Genua M, Bortolomai I, et al. Premature Senescence and Increased Oxidative Stress in the Thymus of Down Syndrome Patients. Front Immunol. 2021;12:1–12.
58. Kizaki H, Tadakuma T. Thymocyte Apoptosis. Microbiol Immunol. 1993;37(12):917–25.
59. Bianchini R, Nocentini G, Krausz LT, Fettucciari K, Coaccioli S, Ronchetti S, et al. Modulation of pro- and antiapoptotic molecules in double-positive (CD4+ CD8+) thymocytes following dexamethasone treatment. J Pharmacol Exp Ther. 2006;319(2):887–97.
60. Van Den Brandt J, Wang D, Reichardt HM. Resistance of Single-Positive Thymocytes to Glucocorticoid-Induced Apoptosis Is Mediated by CD28 Signaling. Mol Endocrinol. 2004;18(3):687–95.
61. Schäcke H, Berger M, Rehwinkel H, Asadullah K. Selective glucocorticoid receptor agonists (SEGRAs): Novel ligands with an improved therapeutic index. Mol Cell Endocrinol. 2007;275(1–2):109–17.
62. Sundahl N, Bridelance J, Libert C, De Bosscher K, Beck IM. Selective glucocorticoid receptor modulation: New directions with non-steroidal scaffolds. Pharmacol Ther. 2015;152:28–41.
63. Meijer OC, Koorneef LL, Kroon J. Glucocorticoid receptor modulators. Ann Endocrinol (Paris). 2018;79(3):107–11.
64. La Motte-Mohs RN, Herer E, Zúniga-Pflücker JC. Induction of T-cell development from human cord blood hematopoietic stem cells by Delta-like 1 in vitro. Blood. 2005;105(4):1431–9.
65. Seet CS, He C, Bethune MT, Li S, Chick B, Gschweng EH, et al. Generation of mature T cells from human hematopoietic stem and progenitor cells in artificial thymic organoids. Nat Methods. 2017;14(5):521–30.
66. Herzstiftung D. Deutscher Herzbericht 2020 [Internet]. 2021. p. 1–196. Available from: https://www.herzstiftung.de/system/files/2021-06/Deutscher-Herzbericht-2020.pdf
67. Gudmundsdottir J, Oskarsdottir S, Skogberg G, Lindgren S, Lundberg V, Berglund M, et al. Early thymectomy leads to premature immunologic ageing: An 18-year follow-up. J Allergy Clin Immunol. 2016;138(5):1439–43.
68. Sauce D, Larsen M, Fastenackels S, Duperrier A, Keller M, Grubeck-Loebenstein B, et al. Evidence of premature immune aging in patients thymectomized during early childhood. J Clin Invest. 2009;119(10):3070–8.
69. van den Broek T, Madi A, Delemarre EM, Schadenberg AWL, Tesselaar K, Borghans JAM, et

al. Human neonatal thymectomy induces altered B-cell responses and autoreactivity. Eur J Immunol. 2017;47(11):1970–81.

70. Gudmundsdottir J, Söderling J, Berggren H, Óskarsdóttir S, Neovius M, Stephansson O, et al. Long-term clinical effects of early thymectomy: Associations with autoimmune diseases, cancer, infections, and atopic diseases. J Allergy Clin Immunol. 2018;141(6):2294–7.
71. Yuki K, Koutsogiannaki S. Neutrophil and T Cell Functions in Patients with Congenital Heart Diseases : A Review. Pediatr Cardiol. 2021;Jul 20:1–5.
72. Williams K, Carson J, Lo C. Genetics of congenital heart disease. Biomolecules. 2019;9(12):1–23.
73. Bruneau BG. The developmental genetics of congenital heart disease. Nature. 2008;451(7181):943–8.
74. Radtke F, Wilson A, Stark G, Bauer M, Van Meerwijk J, MacDonald HR, et al. Deficient T cell fate specification in mice with an induced inactivation of Notch1. Immunity. 1999;10(5):547–58.
75. Davey BT, Elder RW, Cloutier MM, Bennett N, Lee JH, Wang Z, et al. T-Cell Receptor Excision Circles in Newborns with Congenital Heart Disease. J Pediatr. 2019;213:96–102.
76. Liggins GC. The Role of Cortisol in Preparing the Fetus for Birth. Reprod Fertil Dev. 1994;6:141–50.

6 OWN CONTRIBUTION

The underlying idea of my project was developed by my supervisors Eva Tolosa and Anna Gieras. When I joined the working group in 2017, I developed the concepts for the investigations further, identified scientific questions and designed my experiments. All working steps were closely supervised by Eva Tolosa and Anna Gieras. I performed the experiments, analysed the data and contributed to interpretation and discussion.
The technical assistants of our lab, Manuela Kolster, Romy Hackbusch and Nora Kersten, introduced me to the lab work and Manuela Kolster and Romy Hackbusch supported me with tissue preparation, hands on time in the cell culture lab and immunofluorescence staining. Kati Tillack supported me a lot with organisation. Daniel Biermann and Jörg Sachweh provided the thymic tissue and Jörg Sachweh helped me with the classification of the CHD cases.

Regarding the publication, I performed the investigation, the data curation, including sample preparation, staining and FACS-analysis, the formal analysis and the validation and visualization of the data. I helped with project administration and funding acquisition. Additionally, I wrote the original draft of the paper, including the comprehensive supplementary material, as well as the required revisions together with Anna Gieras, supported by Eva Tolosa. Laura Glau did the bioinformatic analysis, especially UMAP analysis performed in R, and helped with visualization of the data. Christina Gehbauer was involved in project administration. Annika Boxnick helped with data curation and validation; she was mainly involved in the extensive revision process and helped with revision experiments. Daniel Biermann and Jörg Sachweh contributed to the resources; especially by providing the thymic tissue from children undergoing corrective cardiac surgery. My supervisors Eva Tolosa and Anna Gieras were responsible for conceptualization, project administration and funding acquisition. They supervised data curation, analysis, validation and visualization. All co-authors contributed to reviewing the manuscript.

7 ACKNOWLEDGEMENTS

First, I would like to thank my “Doktormutter” Professor Eva Tolosa for introducing me to the scientific world and giving me the opportunity to write my thesis in her lab. Thanks Eva for being such a great mentor and for your guidance in professional and personal concerns. I also want to thank Dr. Anna Gieras for her continuous support. Thank you Anna for always having an open ear (especially during the revision process, no matter if it was day- or night-time), for your advice and the countless hours of discussion. I am very grateful for having both of you as teachers.

Special thanks go to the current and former members of the AG Tolosa. Dear Anne, Annika, Arnau, Elena, Enja, Hannah, Hauke, Kati, Laura, Laurenz, Manu, Nora, Riekje, Romy and Sabine, thanks for your boundless help, for showing me how to survive in the lab and for the great time. Manu and Romy, thanks for your patience when introducing me to the lab work and teaching me new methods; Laura, thanks for always helping me with my computer-issues.

I would like to thank all IFIs for the nice working atmosphere and for the new input in many journal clubs and progress reports.

Next, I would like to thank Professor Tiegs and Professor Schramm for supervising me during my year in the Graduate School Programme of the DFG.

Many thanks to our cooperation partners in the Department for Surgery of Congenital Heart Diseases, PD Dr. med. Jörg Sachweh and Dr. med. Daniel Biermann. Thank you for contributing to my exciting research topic, and thank you for the experience on the other side of the operating table during my internship in your department.

Ein herzliches Dankeschön geht an meine Freunde und meine Mitbewohnerin Katja, die stets für Ausgleich und Abwechslung sorgen.

Zuletzt möchte ich mich ganz besonders bei meiner Familie und meinem Freund bedanken. Simon, danke, dass du immer an mich glaubst und für mich da bist. Martien, danke für die Unterstützung und deine Freude über meine Erfolge. Doris, danke, dass du meinen Weg bis hierher ermöglicht hast, dass du mir die Freude am Lernen und die Neugier auf die Wissenschaft gezeigt hast.

8 CURRICULUM VITAE

Lebenslauf wurde aus datenschutzrechtlichen Gründen entfernt.

9 EIDESSTATTLICHE VERSICHERUNG

Ich versichere ausdrücklich, dass ich die Arbeit selbständig und ohne fremde Hilfe verfasst, andere als die von mir angegebenen Quellen und Hilfsmittel nicht benutzt und die aus den benutzten Werken wörtlich oder inhaltlich entnommenen Stellen einzeln nach Ausgabe (Auflage und Jahr des Erscheinens), Band und Seite des benutzten Werkes kenntlich gemacht habe.
Ferner versichere ich, dass ich die Dissertation bisher nicht einem Fachvertreter an einer anderen Hochschule zur Überprüfung vorgelegt oder mich anderweitig um Zulassung zur Promotion beworben habe.
Ich erkläre mich einverstanden, dass meine Dissertation vom Dekanat der Medizinischen Fakultät mit einer gängigen Software zur Erkennung von Plagiaten überprüft werden kann.

Unterschrift: .....